



## Historical Perspective

# Powerful combination of g-C<sub>3</sub>N<sub>4</sub> and LDHs for enhanced photocatalytic performance: A review of strategy, synthesis, and applications



Biao Song<sup>a,1</sup>, Zhuotong Zeng<sup>b,1</sup>, Guangming Zeng<sup>a,\*</sup>, Jilai Gong<sup>a,\*</sup>, Rong Xiao<sup>b,\*</sup>, Shujing Ye<sup>a</sup>, Ming Chen<sup>a</sup>, Cui Lai<sup>a</sup>, Piao Xu<sup>a</sup>, Xiang Tang<sup>a</sup>

<sup>a</sup> College of Environmental Science and Engineering, Hunan University, and Key Laboratory of Environmental Biology and Pollution Control (Hunan University), Ministry of Education, Changsha 410082, PR China

<sup>b</sup> Department of Dermatology, Second Xiangya Hospital, Central South University, Changsha 410011, PR China

## ARTICLE INFO

## Article history:

29 July 2019

Available online 08 August 2019

## Keywords:

Carbon nitride

Layered double hydroxide

2D/2D heterojunction

Photocatalysis

Visible light

## ABSTRACT

The utilization of solar energy with photocatalytic technology has been considered a good solution to alleviate environmental pollution and energy shortage. Constructing 2D/2D heterostructure photocatalysts with layered double hydroxide (LDH) and graphitic carbon nitride (g-C<sub>3</sub>N<sub>4</sub>) is an effective approach to attain high performance in solar photocatalysis. This paper provides a review of recent studies about 2D/2D LDH/g-C<sub>3</sub>N<sub>4</sub> heterostructure photocatalysts. Main strategies for constructing the desired 2D/2D heterojunction are summarized. The planar structure of LDH and g-C<sub>3</sub>N<sub>4</sub> offers a shorter transfer distance for charge carriers and reduces electron-hole recombination in the bulk phase. The face-to-face contact between the two materials can promote the charge transfer across the heterostructure interface, thus improving the electron-hole separation efficiency. The performance and mechanisms of LDH/g-C<sub>3</sub>N<sub>4</sub> photocatalysts in hydrogen production, CO<sub>2</sub> reduction, and organic pollutant degradation are analyzed and discussed. Incorporating reduced graphene oxide or Ag nanoparticles into LDH/g-C<sub>3</sub>N<sub>4</sub> heterojunction and fabricating calcined LDH/g-C<sub>3</sub>N<sub>4</sub> composites are effective strategies to further facilitate charge transfer at the interface of LDH and g-C<sub>3</sub>N<sub>4</sub> and improve the absorption capacity for visible light. This review is expected to provide basic insights into the design of 2D/2D LDH/g-C<sub>3</sub>N<sub>4</sub> heterojunctions and their applications in solar photocatalysis.

© 2019 Elsevier B.V. All rights reserved.

## Contents

1. Introduction	2
2. Characteristics of 2D/2D LDH/g-C <sub>3</sub> N <sub>4</sub> as photocatalysts	2
3. Construction of 2D/2D LDH/g-C <sub>3</sub> N <sub>4</sub> heterojunctions	2
3.1. Electrostatic self-assembly	2
3.2. In-situ coprecipitation	4
3.3. Hydrothermal method	4
3.4. Solvothermal method	5
3.5. Calcination method	5
4. Applications of LDH/g-C <sub>3</sub> N <sub>4</sub> photocatalytic systems	7
4.1. LDH/g-C <sub>3</sub> N <sub>4</sub> binary photocatalysts	7
4.2. LDH/g-C <sub>3</sub> N <sub>4</sub> /X ternary photocatalysts	10
4.3. Calcined LDH/g-C <sub>3</sub> N <sub>4</sub> photocatalysts	12
5. Conclusion and outlook	14
Acknowledgements	15
References	15

\* Corresponding authors.

E-mail addresses: [zgming@hnu.edu.cn](mailto:zgming@hnu.edu.cn) (G. Zeng), [jilaigong@hnu.edu.cn](mailto:jilaigong@hnu.edu.cn) (J. Gong), [xiaorong65@csu.edu.cn](mailto:xiaorong65@csu.edu.cn) (R. Xiao).

<sup>1</sup> These authors contribute equally to this article.

## 1. Introduction

Environmental pollution and energy shortage have brought great challenges to human sustainable development [1–6]. Exploiting clean and renewable solar energy with photocatalytic technology has been widely considered one of promising solutions to the problems [7–12]. Photocatalytic technology can utilize solar irradiation to realize organic pollutant degradation [13,14], Cr(VI) reduction [15,16], and bacterial inactivation [17,18], which provides a great way for pollution abatement. Additionally, considerable effort is being directed at photocatalytic hydrogen production and CO<sub>2</sub> reduction for converting solar energy to chemical energy [19–22]. If this technology can be applied in large scale, the energy crisis will be effectively alleviated. Photocatalytic reaction is essentially a photoinduced redox process. Photocatalyst is the core of photocatalytic technology, and plays a vital role in harvesting light and driving the reaction [23–26]. Thus, the study of high-efficient photocatalyst is essential for the development of photocatalytic technology.

Graphitic carbon nitride (g-C<sub>3</sub>N<sub>4</sub>) is a polymer semiconductor with triazine or heptazine as a basic structural unit, and has a graphite-like layer structure [27,28]. Since its application in photocatalytic hydrogen production was first reported [29], g-C<sub>3</sub>N<sub>4</sub> has attracted wide attention and been extensively researched for photocatalytic applications [30–33]. Compared with conventional photocatalysts (e.g., TiO<sub>2</sub>), the band gap of g-C<sub>3</sub>N<sub>4</sub> is smaller (~2.7 eV), which allows it to function under visible light [33]. Additionally, the great chemical stability, high thermostability, cheap raw materials, and simple synthesis process make g-C<sub>3</sub>N<sub>4</sub> competitive among various photocatalytic materials [30]. Nevertheless, g-C<sub>3</sub>N<sub>4</sub> faces many problems in its practical applications. Only blue and violet light (wavelength < 460 nm) can be absorbed by g-C<sub>3</sub>N<sub>4</sub>, which causes low utilization rate of solar energy [34]. Fast recombination of photoinduced electron-hole pairs in g-C<sub>3</sub>N<sub>4</sub> decreases the redox ability [35]. The bulk structure of g-C<sub>3</sub>N<sub>4</sub> leads to relatively small specific surface area [36]. These shortcomings limit the further development of g-C<sub>3</sub>N<sub>4</sub> for photocatalytic applications. Many strategies have been used to improve the photocatalytic activity of g-C<sub>3</sub>N<sub>4</sub>, such as loading co-catalyst, doping element (e.g., Fe, Zn, P, and S), designing nanostructure, and constructing heterojunction [37–40]. Among these strategies, constructing heterostructure with other semiconductor materials is typically applied to facilitate the separation of charge carriers in g-C<sub>3</sub>N<sub>4</sub>. Due to the difference in Fermi level of two different semiconductors, charge carriers can move between the semiconductors when they contact with each other, which finally forms an internal electric field at the interface. The photoinduced electrons and holes can move directionally in the electric field, thus being separated effectively [41].

Recently, using layered double hydroxides (LDHs) to construct heterojunction with g-C<sub>3</sub>N<sub>4</sub> has been found a highly effective strategy for enhancing the photocatalytic performance. LDHs are a class of two-dimensional (2D) materials of hydroxide-like clays, which are composed of positively charged host layers and exchangeable interlayer anions. They can be expressed by a general chemical formula [M<sub>1</sub><sup>2+</sup><sub>1-x</sub>M<sub>x</sub><sup>3+</sup>(OH)<sub>2</sub>](A<sup>n-</sup>)<sub>x/n</sub>·mH<sub>2</sub>O, where M<sup>2+</sup> is divalent cation (e.g., Ca<sup>2+</sup>, Co<sup>2+</sup>, Fe<sup>2+</sup>, Mg<sup>2+</sup>, Ni<sup>2+</sup>, and Zn<sup>2+</sup>), M<sup>3+</sup> is trivalent cation (e.g., Al<sup>3+</sup>, Co<sup>3+</sup>, Cr<sup>3+</sup>, Fe<sup>3+</sup>, Mn<sup>3+</sup>, and Ni<sup>3+</sup>), A<sup>n-</sup> is interlayer anion (e.g., CO<sub>3</sub><sup>2-</sup>, SO<sub>4</sub><sup>2-</sup>, NO<sub>3</sub><sup>-</sup>, and Cl<sup>-</sup>), x is the molar ratio of trivalent cation in total cations [M<sup>3+</sup> / (M<sup>2+</sup> + M<sup>3+</sup>)], and m is the crystal water number for each LDH molecule [42,43]. Due to the low cost, high chemical stability, adjustable composition and uniform distribution of metal cations, as well as exchangeable interlayer anions, LDHs and their calcined products have found applications in many fields including photocatalysis [44]. However, pure LDHs are dissatisfactory in photocatalytic processes due to the fast recombination of photoinduced electron-hole pairs [43]. Constructing LDH/g-C<sub>3</sub>N<sub>4</sub> heterojunctions with clever design can overcome the disadvantages of g-C<sub>3</sub>N<sub>4</sub> and LDHs, and obtain ideal photocatalysts with excellent performance. In this article, recent advances in 2D/2D LDH/g-C<sub>3</sub>N<sub>4</sub> heterostructure photocatalysts

and their applications for solar energy conversion and pollution abatement are carefully reviewed. The characteristics of 2D/2D LDH/g-C<sub>3</sub>N<sub>4</sub> as photocatalysts are first summarized to provide better understanding of the strategy for constructing LDH/g-C<sub>3</sub>N<sub>4</sub> heterostructures. Then, various methods to achieve effective assembly of LDH and g-C<sub>3</sub>N<sub>4</sub> are introduced and discussed. The applications of LDH/g-C<sub>3</sub>N<sub>4</sub> photocatalytic systems in H<sub>2</sub> production, CO<sub>2</sub> reduction, and organic pollutant degradation are reviewed and analyzed. Lastly, some future research needs in 2D/2D LDH/g-C<sub>3</sub>N<sub>4</sub> heterostructure photocatalysts are proposed. This work may benefit the design of high-efficient LDH/g-C<sub>3</sub>N<sub>4</sub> photocatalysts and their applications.

## 2. Characteristics of 2D/2D LDH/g-C<sub>3</sub>N<sub>4</sub> as photocatalysts

Constructing 2D/2D heterostructure has been considered an effective way to enhance the photocatalytic activity of LDH/g-C<sub>3</sub>N<sub>4</sub> composites. The 2D structure of LDHs and g-C<sub>3</sub>N<sub>4</sub> offers plentiful surface active sites for constructing photocatalytic composites and substantially shortens the transfer distance of photoinduced charge carriers within the materials, which is advantageous to the photocatalytic reactions [45–48]. The tunable composition and band structure make LDHs excellent semiconductors for constructing photocatalytic heterojunctions with g-C<sub>3</sub>N<sub>4</sub>. By adjusting and controlling the M<sup>2+</sup> and M<sup>3+</sup> in LDHs, the band gap of LDHs can be in the range of 2.0–3.4 eV, which benefits the harvesting of visible light [49]. Abundant basic sites on LDHs enable the materials to be used as heterogeneous solid base catalysts for many chemical reactions, and the position of catalytic active sites and product selectivity are also tunable as the metal cations and interlayer anions can be artificially controlled [50,51]. Additionally, it is relatively easy to design the number of layers and interlayer space of LDHs, and functionalize LDHs with g-C<sub>3</sub>N<sub>4</sub> [47,52]. Constructing 2D/2D heterostructure with LDHs and g-C<sub>3</sub>N<sub>4</sub> can make good use of the photocatalytic characteristics of these two 2D materials. Compared with other types of photocatalysts, 2D/2D LDH/g-C<sub>3</sub>N<sub>4</sub> heterostructure has many advantages (Fig. 1). (1) Because of face-to-face contact between the two semiconductors, photoinduced charge carriers can transfer more efficiently across the heterojunction interface, which is conducive to electron-hole separation in a single material [53,54]. (2) The 2D LDHs and g-C<sub>3</sub>N<sub>4</sub> have a higher surface area that can increase the contact between photocatalyst and reaction substrate, as well as the light harvesting ability of the photocatalyst [55,56]. (3) 2D/2D heterostructure takes advantage of short transfer distance of charge carriers within LDHs and g-C<sub>3</sub>N<sub>4</sub>, and decreases the electron-hole recombination in the bulk phase [57,58]. (4) The band structure of 2D/2D LDH/g-C<sub>3</sub>N<sub>4</sub> heterostructure is tunable, which makes the photocatalyst suitable for various application systems [59–61]. These merits greatly improve the photocatalytic performance and applications of 2D/2D LDH/g-C<sub>3</sub>N<sub>4</sub> heterojunctions.

## 3. Construction of 2D/2D LDH/g-C<sub>3</sub>N<sub>4</sub> heterojunctions

The design and synthesis of photocatalyst are of great importance to achieve a good photocatalytic performance. Based on the assembly strategies of LDHs and g-C<sub>3</sub>N<sub>4</sub> and the desired 2D/2D structure, the constructing methods mainly include electrostatic self-assembly, in-situ coprecipitation, hydrothermal method, solvothermal method, and calcination method. The following sections provide detailed information about these synthesis methods.

### 3.1. Electrostatic self-assembly

Electrostatic self-assembly is commonly used for constructing layered composites. It makes use of the electrostatic interaction between differently charged materials [62]. In the self-assembly process, the electrostatic attraction between opposite charges mainly drives the assembly, and meanwhile the assembly of each layer is controlled due

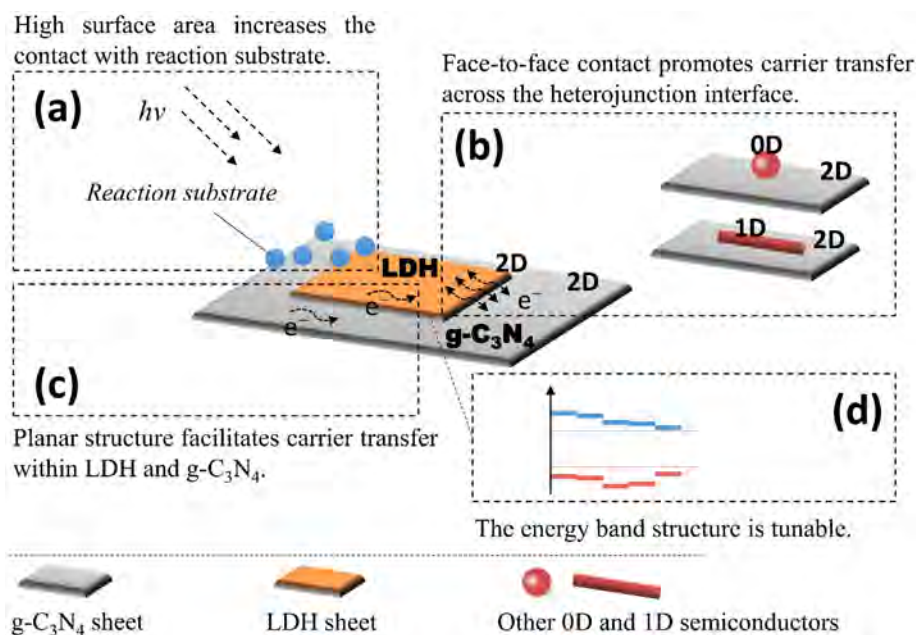


Fig. 1. Advantages of 2D/2D LDH/g-C<sub>3</sub>N<sub>4</sub> heterostructure in photocatalytic applications.

to the electrostatic repulsion between like charges. This method has been successfully applied in synthesizing many 2D/2D photocatalysts [62–65]. The water suspension of pristine g-C<sub>3</sub>N<sub>4</sub> is negatively charged because of the amine-group deprotonation [66], while the host layer of LDHs is positively charged because of the ordered arrangement of metal cations [67]. These properties provide the basis for constructing LDH/g-C<sub>3</sub>N<sub>4</sub> heterojunctions via electrostatic self-assembly. In the synthesis process, LDH and g-C<sub>3</sub>N<sub>4</sub> are generally synthesized and exfoliated to sheets separately before the self-assembly. Many methods for exfoliating LDHs through ultrasonic treatment or mechanical stirring have been reported, such as directly exfoliating LDHs in organic solvents (e.g., formamide), and exfoliating LDHs after they are intercalated with organic anions (e.g., dodecyl benzene sulfonate) [68]. Additionally, LDHs can also be exfoliated through hydrothermal method, and the key to effectively delaminate LDHs is that the LDHs must be newly prepared wet sample [69]. In the laboratory, photocatalytic g-C<sub>3</sub>N<sub>4</sub> nanosheets are mainly obtained through sonication exfoliation of bulk g-C<sub>3</sub>N<sub>4</sub> [70,71].

Hong et al. [72] synthesized Mg-Al-LDH/g-C<sub>3</sub>N<sub>4</sub> photocatalyst by electrostatic self-assembly (Fig. 2). In that study, the authors first synthesized g-C<sub>3</sub>N<sub>4</sub> from urea by thermal polymerization and Mg-Al-LDH by precipitation with NaOH. Then, the g-C<sub>3</sub>N<sub>4</sub> nanosheets and Mg-Al-LDH nanosheets were obtained through sonication exfoliation and

hydrothermal method. According to the measurement, the obtained g-C<sub>3</sub>N<sub>4</sub> suspension and Mg-Al-LDH suspension had a zeta potential of  $-27.3$  mV and  $+52.7$  mV, respectively. By directly mixing the two suspensions, the g-C<sub>3</sub>N<sub>4</sub> nanosheets and Mg-Al-LDH nanosheets assembled via electrostatic interaction and Mg-Al-LDH/g-C<sub>3</sub>N<sub>4</sub> photocatalyst was obtained. For confirming the 2D/2D assembly of Mg-Al-LDH and g-C<sub>3</sub>N<sub>4</sub>, the authors observed the photocatalyst morphology by transmission electron microscope (TEM), and found that Mg-Al-LDH flakes were well distributed on g-C<sub>3</sub>N<sub>4</sub> sheets. Nayak et al. [73] reported a weight impregnation method for synthesizing Ni-Fe-LDH/g-C<sub>3</sub>N<sub>4</sub> composite. It is actually a self-assembly process via electrostatic interaction, but the process was somewhere different from the above one. In their experiments, Ni-Fe-LDH and g-C<sub>3</sub>N<sub>4</sub> were first produced by coprecipitation method and thermal polymerization, respectively. When synthesizing the Ni-Fe-LDH, the NaOH solution was dropwise added and the resulting precipitate was vigorously stirred for 24 h, in order to obtain Ni-Fe-LDH easy to be exfoliated in the following procedure. Then, the obtained Ni-Fe-LDH and g-C<sub>3</sub>N<sub>4</sub> were severally suspended in methanol and ultrasonically treated for 30 min to obtain nanosheet suspensions. The two suspensions were subsequently mixed and put in a fume cupboard to completely volatilize methanol and obtain the final product. Though electrostatic self-assembly offers a simple operation for constructing LDH/g-C<sub>3</sub>N<sub>4</sub> photocatalyst, the

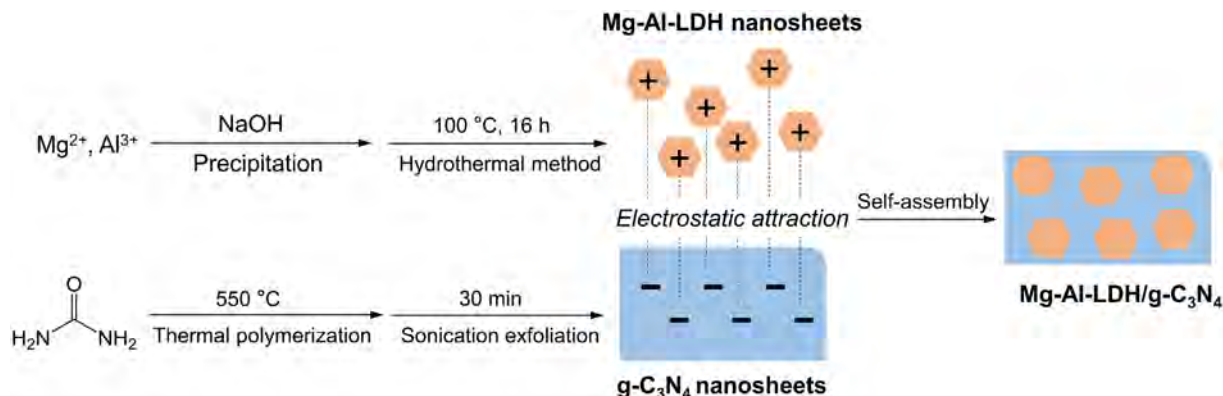


Fig. 2. Synthesis of Mg-Al-LDH/g-C<sub>3</sub>N<sub>4</sub> photocatalyst by electrostatic self-assembly. This schematic diagram was drawn according to the method used by Hong et al. [72].

assembly process is difficult to control and it is affected by many factors, such as material surface roughness and effective charges. Therefore, using this method alone for LDH/g-C<sub>3</sub>N<sub>4</sub> synthesis was relatively few. However, the electrostatic interaction between LDHs and g-C<sub>3</sub>N<sub>4</sub> was also involved in constructing LDH/g-C<sub>3</sub>N<sub>4</sub> photocatalyst with many other methods.

### 3.2. In-situ coprecipitation

Coprecipitation is the simultaneous precipitation of two or more cations in a homogeneous solution by adding a precipitating agent. This method has been an important way to synthesize composites that contain two or more metals, due to the simple operation, low cost, manageable reaction conditions, short synthesis time, and good products with uniform composition [74–76]. Coprecipitation is also a commonly used method for synthesizing LDHs [77]. The desired LDHs can be obtained by adding alkaline liquor into the mixed solution of metal cations that are needed for the host layer and subsequent aging of the resulting suspension. The mixed cation solution or the alkaline liquor contains interlayer anions of the LDHs. The LDH size can be tuned through changing the reaction conditions such as solution pH value, temperature, and aging time. For constructing LDH/g-C<sub>3</sub>N<sub>4</sub> by coprecipitation, the basic strategy is to precipitate the metal cations in situ after they are adsorbed on the g-C<sub>3</sub>N<sub>4</sub> sheet via electrostatic attraction.

Liu et al. [56] successfully synthesized 2D/2D Zn-Cr-LDH/g-C<sub>3</sub>N<sub>4</sub> heterojunction by in-situ coprecipitation. Fig. 3 illustrates the specific synthesis process. The authors first synthesized modified g-C<sub>3</sub>N<sub>4</sub> sheets from urea in the presence of citric acid (denoted as g-C<sub>3</sub>N<sub>4</sub>-C(N) by the authors) and made them to a suspension. Then, Zn<sup>2+</sup> and Cr<sup>3+</sup> were added to the suspension with stirring. In this process, Zn<sup>2+</sup> and Cr<sup>3+</sup> were adsorbed on the g-C<sub>3</sub>N<sub>4</sub>-C(N) sheet through electrostatic attraction. NaOH was subsequently added to precipitate Zn<sup>2+</sup> and Cr<sup>3+</sup> and form Zn-Cr-LDH in situ on g-C<sub>3</sub>N<sub>4</sub> surface. The authors further applied the Zn-Cr-LDH/g-C<sub>3</sub>N<sub>4</sub>-C(N) product for photocatalytic degradation of Congo red, and the photocatalytic activity was higher than that with Zn-Cr-LDH or g-C<sub>3</sub>N<sub>4</sub> as the photocatalyst. Arif et al. [78] synthesized Co-Mn-LDH/g-C<sub>3</sub>N<sub>4</sub> heterojunction by a similar in-situ coprecipitation process. In the experimental section of their report, it was emphasized

that the mixture of metal cations and g-C<sub>3</sub>N<sub>4</sub> needed to be ultrasonically treated for over one hour to enable sufficient adsorption of Co<sup>2+</sup> and Mn<sup>2+</sup> on g-C<sub>3</sub>N<sub>4</sub> sheets through electrostatic interaction. This treatment process is vital to ensure an effective in-situ coprecipitation. Yuan and Li [79] reported an in-situ crystallization method for fabricating Zn-Al-LDH/g-C<sub>3</sub>N<sub>4</sub> composites. It is actually an in-situ coprecipitation process. In that study, Zn-Al-LDH crystals formed in situ on g-C<sub>3</sub>N<sub>4</sub> sheets as the coprecipitation of Zn<sup>2+</sup> and Al<sup>3+</sup>. The authors observed the microstructure of Zn-Al-LDH/g-C<sub>3</sub>N<sub>4</sub> by TEM and found that relatively large g-C<sub>3</sub>N<sub>4</sub> sheet was uniformly covered with Zn-Al-LDH flakes. It was considered that g-C<sub>3</sub>N<sub>4</sub> could act as a substrate to induce the LDH crystallite growth. Polar functional groups on g-C<sub>3</sub>N<sub>4</sub> had a good affinity for metal cations, which was conducive to the enrichment of Zn<sup>2+</sup> and Al<sup>3+</sup> and the growth of Zn-Al-LDH crystals on the g-C<sub>3</sub>N<sub>4</sub> sheets. According to these studies, electrostatic interaction and g-C<sub>3</sub>N<sub>4</sub>-induced crystallization are the main mechanisms of LDH/g-C<sub>3</sub>N<sub>4</sub> synthesis by in-situ coprecipitation.

### 3.3. Hydrothermal method

Hydrothermal method, also termed hydrothermal synthesis, is a common technique for producing composite materials via chemical reactions that occur in aqueous solution in a pressure-tight reactor with high temperature and high pressure [80]. The main advantage of this method is that well-crystallized product can be easily obtained by a simple hydrothermal process [81]. Additionally, it is convenient to design the product morphology and structure through controlling the reaction conditions [82]. According to the reaction type, hydrothermal method can be further divided into hydrothermal oxidation, hydrothermal reduction, hydrothermal precipitation, hydrothermal decomposition, hydrothermal polymerization, and so on. For constructing LDH/g-C<sub>3</sub>N<sub>4</sub> heterostructure, hydrothermal precipitation method was used in many studies. Some metal cations are difficult to form layered hydroxides by coprecipitation under mild temperature and pressure conditions, but the reaction is easier to occur in a hydrothermal system with high temperature and pressure. Furthermore, the resulting LDH/g-C<sub>3</sub>N<sub>4</sub> products usually have a good 2D/2D morphology.

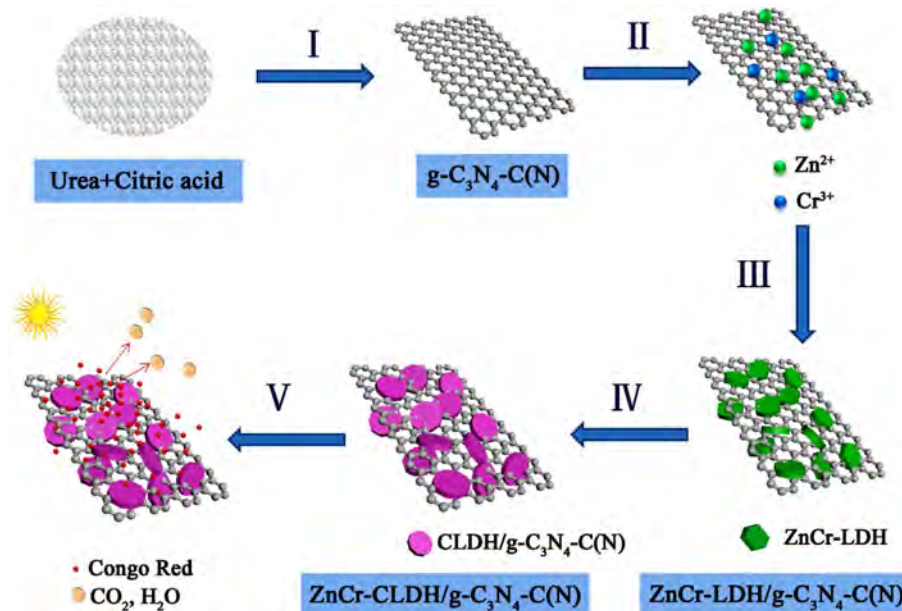


**Fig. 3.** Schematic illustration of the fabrication route of hybrid Zn-Cr-CLDH/g-C<sub>3</sub>N<sub>4</sub>-C(N) nanocomposites. (I) Thermal polymerization at 550 °C; (II) adding Zn<sup>2+</sup> and Cr<sup>3+</sup> under stirring; (III) in situ precipitation of Zn-Cr-LDH on g-C<sub>3</sub>N<sub>4</sub>-C(N); (IV) calcinations and formation of Zn-Cr-CLDH/g-C<sub>3</sub>N<sub>4</sub>-C(N); (V) adsorption and photocatalytic Congo red under visible light. Reproduced with permission from ref. [56]. Copyright 2018 Elsevier. (For interpretation of the references to colour in this figure legend, the reader is referred to the web version of this article.)

Liu et al. [83] synthesized Zn-Cr-LDH/g-C<sub>3</sub>N<sub>4</sub> composite by a hydrothermal method (Fig. 4). In their experiments, g-C<sub>3</sub>N<sub>4</sub> nanosheet suspension was obtained through ultrasonic treatment of bulk g-C<sub>3</sub>N<sub>4</sub>, which was prepared through thermal polymerization with urea as the raw material. Then, Zn<sup>2+</sup>, Cr<sup>3+</sup>, and alkaline liquor (NaOH and Na<sub>2</sub>CO<sub>3</sub>) were added to the suspension. The hydrothermal reaction was carried out in a Teflon-lined stainless steel autoclave at 120 °C for 24 h. The Zn-Cr-LDH/g-C<sub>3</sub>N<sub>4</sub> product was finally obtained by collecting and drying the precipitates from the autoclave. For constructing LDH/g-C<sub>3</sub>N<sub>4</sub> photocatalysts with a better 2D/2D morphology, Wu et al. [54] used urea and NH<sub>4</sub>F instead of NaOH alkaline liquor in the hydrothermal synthesis of Co-Al-LDH/O-doped g-C<sub>3</sub>N<sub>4</sub>. In this process, the hydrolysis of urea was utilized to precipitate Co<sup>2+</sup> and Al<sup>3+</sup>, which avoided the unevenness of LDH size resulting from the nonuniform precipitant distribution and reaction rate. Urea broke down into NH<sub>3</sub> and CO<sub>2</sub> by hydrolysis. The generated NH<sub>3</sub> increased the pH value of reaction mixture, while the release of CO<sub>2</sub> played a role of agitation. Thus, homogeneous precipitation of Co-Al-LDH flakes gradually occurred, and the products were of high purity and uniform size. Considering the difficulty in recycling powder photocatalysts from aqueous solutions in practical applications, Yazdani et al. [84] fabricated a Ni-Ti-LDH/g-C<sub>3</sub>N<sub>4</sub> heterojunction film by hydrothermal method and used it as a fix-bed photoreactor. In their experiments, g-C<sub>3</sub>N<sub>4</sub> film was first synthesized on a quartz glass substrate via thermal polymerization, and then the g-C<sub>3</sub>N<sub>4</sub>-covered substrate was further used to load Ni-Ti-LDH film by hydrothermal treatment. The formation of Ni-Ti-LDH was achieved by precipitation through urea hydrolysis. Layered structure of LDH and g-C<sub>3</sub>N<sub>4</sub> makes them suitable for constructing 2D photocatalytic films. Using immobilized LDH/g-C<sub>3</sub>N<sub>4</sub> photocatalyst may benefit its practical applications in aqueous solutions.

#### 3.4. Solvothermal method

Solvothermal method is further developed from hydrothermal method. It uses organic solvents as reaction media. Despite many advantages of hydrothermal method, it is limited in synthesizing some non-oxides (e.g., carbides, nitrides, and phosphides) as the reactants and products may react with water, hydrolyze, or be unstable in water [85]. Using nonaqueous solvents can help to run these reactions successfully. Additionally, many properties of organic solvent

(e.g., density, viscosity, and surface tension) vary a lot under high-pressure condition, which can provide special media for many chemical reactions [86]. At the same temperature, the gas pressure in solvothermal system can reach a higher level compared with that in hydrothermal system due to the lower boiling point of some organic solvents, and the high pressure favors the product crystallization [87]. For constructing LDH/g-C<sub>3</sub>N<sub>4</sub> heterostructure, organic solvent can improve the dispersity of reaction precursors (e.g., g-C<sub>3</sub>N<sub>4</sub> suspension), which increases the chemical reactivity and facilitates the construction of 2D/2D structure. Considering the advantages, solvothermal method was applied for synthesizing LDH/g-C<sub>3</sub>N<sub>4</sub> photocatalysts in many studies.

Zhang et al. [88] synthesized Zn-Al-LDH/g-C<sub>3</sub>N<sub>4</sub> composites by solvothermal method. In their experiments, ethylene glycol (EG) served as the reaction medium (Fig. 5). The g-C<sub>3</sub>N<sub>4</sub> was prepared by calcining urea and suspended in EG with NaOH. Metal salts were added into another EG. The two EG suspensions were then mixed for the solvothermal treatment. According to the TEM observation, g-C<sub>3</sub>N<sub>4</sub> sheets were well dispersed in EG and the Zn-Al-LDH/g-C<sub>3</sub>N<sub>4</sub> products exhibited a satisfactory layered structure. Additionally, due to the intercalation of EG in the solvothermal reaction, the interlayer distance of Zn-Al-LDH (1.03 nm) was found larger than that of conventional LDHs intercalated with carbonate (0.73 nm). A relatively large interlayer space can provide more space for reactant diffusion and more active sites for photocatalytic reaction, which helps to increase the photocatalytic efficiency [89,90]. Shakeel et al. [91] used a mixed solvent of water and methanol for constructing Ni-Mn-LDH/g-C<sub>3</sub>N<sub>4</sub> composite. To obtain a stable g-C<sub>3</sub>N<sub>4</sub> nanosheet suspension, the g-C<sub>3</sub>N<sub>4</sub> was ultrasonically treated in the mixed solvent before being transferred to the solvothermal reactor. Similar operation was performed with a mixed solvent of water and dimethylformamide (DMF) by Arif et al. [92] in synthesizing Co-Fe-LDH/g-C<sub>3</sub>N<sub>4</sub> composite. With the assistance of these organic solvents, the dispersity of g-C<sub>3</sub>N<sub>4</sub> sheets was greatly improved, which contributed to the synthesis of products with high quality.

#### 3.5. Calcination method

Calcination is a thermal treatment process in which a substance is heated to lose water or undergo redox reactions. This method is applied

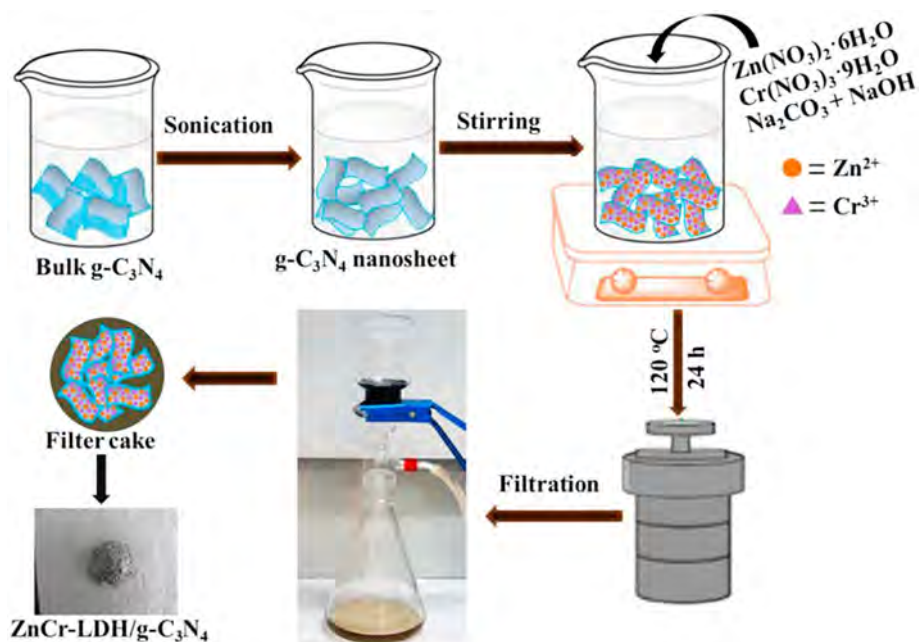


Fig. 4. Schematic representation of the synthesis process of the Zn-Cr-LDH/g-C<sub>3</sub>N<sub>4</sub> composite. Reproduced with permission from ref. [83]. Copyright 2018 Elsevier.

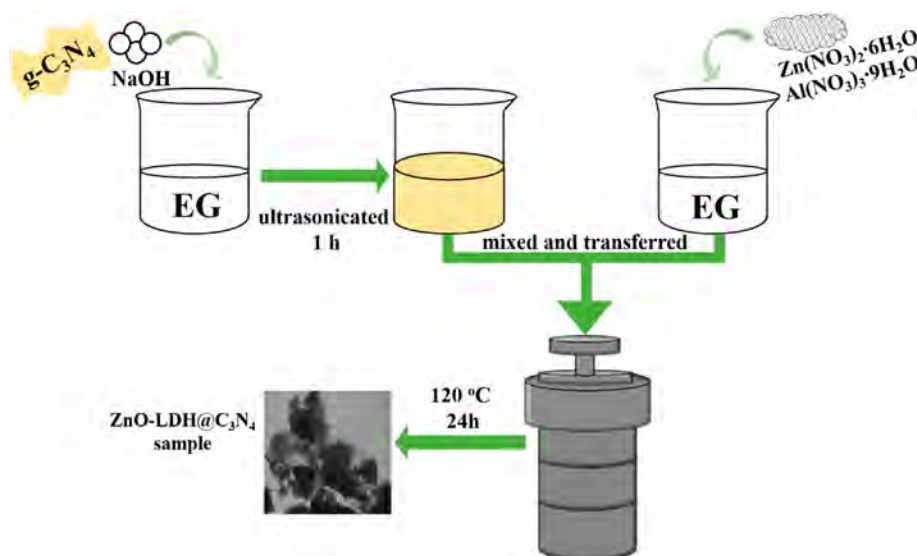


Fig. 5. Schematic representation of the synthesis process of the Zn-Al-LDH/g-C<sub>3</sub>N<sub>4</sub> composite. Reproduced with permission from ref. [88]. Copyright 2016 The Authors.

for synthesizing calcined LDH/g-C<sub>3</sub>N<sub>4</sub> composites. In the synthesis process, LDHs are used as precursors and calcined to form mixed metal oxides (MMOs) via topological transformation [93,94]. The resulting MMOs can be highly dispersed and have a good thermal stability. Due to the formation of metal oxides with higher porosity and specific surface area, the photocatalytic activity can be further improved [95]. Additionally, the calcination of LDHs may generate spinels that can help to increase the harvesting ability for visible light [96,97]. According to the available literature, there are three calcination strategies to obtain calcined LDH/g-C<sub>3</sub>N<sub>4</sub> composites. The first way is directly calcining prepared LDH/g-C<sub>3</sub>N<sub>4</sub> composites [98]. The second method is calcining LDH to MMO, followed by a secondary calcination of the mixture of MMO and g-C<sub>3</sub>N<sub>4</sub> raw material [60]. The third approach is calcining the mixture of LDH and g-C<sub>3</sub>N<sub>4</sub> raw material together, and this method was more widely used [96,97,99,100]. Fig. 6 illustrates the

synthesis of calcined Zn-Fe-LDH/g-C<sub>3</sub>N<sub>4</sub> composites through calcining the mixture of Zn-Fe-LDH and melamine together by Di et al. [97]. In the experiment, Zn-Fe-LDH was first synthesized by hydrothermal treatment. Urea hydrolysis was utilized to achieve homogeneous precipitation of Zn<sup>2+</sup> and Fe<sup>3+</sup>. Melamine simultaneously underwent the hydrothermal treatment to dissolve and recrystallize after cooling down. The resulting precipitates were then calcined at 550 °C to produce the calcined Zn-Fe-LDH/g-C<sub>3</sub>N<sub>4</sub> composites. The calcination temperature was relatively higher than that in directly calcining prepared LDH/g-C<sub>3</sub>N<sub>4</sub> composites (300 °C), because the synthesis of g-C<sub>3</sub>N<sub>4</sub> needed to be simultaneously accomplished during the topological transformation of LDH to MMO [98]. An attractive property of LDHs is the structural memory effect that many LDH-derived MMOs generated at moderate calcination temperature (generally below 500 °C) can reconstruct the LDHs by being added to the solution that contains desired



Fig. 6. (a) Schematic illustration of synthesizing the calcined Zn-Fe-LDH/g-C<sub>3</sub>N<sub>4</sub> composites; photographs of the g-C<sub>3</sub>N<sub>4</sub> (b), the calcined Zn-Fe-LDH (c), and the calcined Zn-Fe-LDH/g-C<sub>3</sub>N<sub>4</sub> products with different weight percentages of g-C<sub>3</sub>N<sub>4</sub> (d-h, from left to right: 0.5, 1.0, 5.0, 70, and 90 wt%). Reproduced with permission from ref. [97]. Copyright 2018 Elsevier.

anions [101,102]. This property is conducive to LDHs as adsorbents for removing anionic pollutants from wastewater [93]. However, the memory effect should be abandoned in order to make full use of the photocatalytic capacity of calcined LDHs, as the formation of spinels at high calcination temperature will destroy the structural memory effect [103]. For example, Mg-Al-LDH would generate  $MgAl_2O_4$  spinel at a calcination temperature over 600 °C [104]. Therefore, it is important to control the calcination temperature when synthesizing calcined LDH/g- $C_3N_4$  composites for photocatalytic applications.

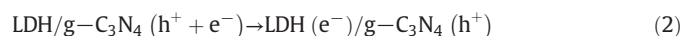
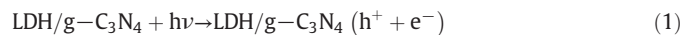
#### 4. Applications of LDH/g- $C_3N_4$ photocatalytic systems

Rational design of 2D/2D structure can considerably enhance the performance of LDH/g- $C_3N_4$  photocatalysts, which enables them to be widely used for energy and environmental applications based on solar photocatalysis. The photocatalytic applications mainly involve hydrogen production from water splitting,  $CO_2$  reduction, and organic pollutant degradation. The performance and mechanism of various LDH/g- $C_3N_4$  photocatalysts are reviewed and discussed in this section.

##### 4.1. LDH/g- $C_3N_4$ binary photocatalysts

According to available literature, divalent cations including  $Co^{2+}$ ,  $Mg^{2+}$ ,  $Ni^{2+}$ , and  $Zn^{2+}$ , and trivalent cations including  $Al^{3+}$ ,  $Cr^{3+}$ ,  $Fe^{3+}$ ,  $Mn^{3+}$ , and  $Ti^{3+}$  were used to construct LDH/g- $C_3N_4$  binary photocatalysts (Table 1). These LDH/g- $C_3N_4$  photocatalysts with improved photocatalytic activity were explored for solar energy conversion and pollution abatement. Nayak et al. [73] fabricated Ni-Fe-LDH/g- $C_3N_4$  composites with various g- $C_3N_4$  content (2, 5, 8, 10, 12, and 15 wt%, denoted as CNLDH2, CNLDH5, CNLDH8, CNLDH10, CNLDH12, and CNLDH15 by the authors, respectively) and applied them for water splitting. Fig. 7a and b showed the evolution amount of  $H_2$  and  $O_2$  with different photocatalysts during two-hour irradiation process with visible light. The CNLDH10 composite presented the highest photocatalytic performance for water splitting and the evolution amounts of  $H_2$  and  $O_2$  were 1488 and 886  $\mu\text{mol/g}$ , respectively. The combination of Ni-Fe-LDH and 10 wt% g- $C_3N_4$  greatly enhanced water splitting efficiency compared with that by only Ni-Fe-LDH or g- $C_3N_4$ . The reduced electron-hole recombination mainly contributed to the result. According to experimental results, the photoluminescence (PL) intensity was negatively related to photocatalytic activity (Fig. 7c). The PL was excited when the electrons and holes recombined, thus the PL spectra suggested that coupling Ni-Fe-LDH and g- $C_3N_4$  could efficiently separate photoinduced charge carriers and decrease their recombination. In the water splitting process, both Ni-Fe-LDH and g- $C_3N_4$  could produce electron-hole pairs with visible light irradiation. As the conduction band (CB) edge potential of g- $C_3N_4$  is more negative than that of Ni-Fe-LDH, the photoinduced electrons on g- $C_3N_4$  could move to the CB

of Ni-Fe-LDH. The electrons ( $e^-$ ) on the CB of Ni-Fe-LDH were captured by  $H^+$  to generate  $H_2$ . Similarly, the holes ( $h^+$ ) on the valence band (VB) of Ni-Fe-LDH could move to the VB of g- $C_3N_4$  where the holes oxidized  $H_2O$  to form  $O_2$  (Fig. 7d). The photocatalytic process can be explained with the following equations:



Apart from being directly used as powder photocatalysts, LDH/g- $C_3N_4$  composites have also been studied as electrode materials of photoelectrochemical cell (PEC), which can convert solar energy to electric energy for water splitting. The hydrogen and oxygen evolve at the cathode and anode, respectively. Water splitting by PEC can utilize electrode as the photocatalyst support, which simplifies the separation of photocatalyst from water and favors the recycling of photocatalyst. Additionally, the electron-hole recombination can be suppressed by bias voltage. Arif et al. [92] constructed Co-Fe-LDH/g- $C_3N_4$  composite and used it as both the anode and the cathode in a two-electrode electrolyzer for overall water splitting. Their results suggested that the Co-Fe-LDH/g- $C_3N_4$  composite could enhance the current density at a lower over potential compared with pristine Co-Fe-LDH and g- $C_3N_4$ . The improved photoelectrocatalytic performance in water splitting mainly resulted from the suppressed electron-hole recombination in Co-Fe-LDH/g- $C_3N_4$  and its 2D/2D porous structure that provided higher active surface area for gas penetration and release. These examples both demonstrate that LDH/g- $C_3N_4$  composites can display a higher photocatalytic performance in water splitting through the construction of 2D/2D structure and rational ratio control, and the enhanced performance is mainly due to the decreased electron-hole recombination in the heterojunction.

Tonda et al. [53] constructed 2D/2D Ni-Al-LDH/g- $C_3N_4$  composites with various weight percentages of Ni-Al-LDH (5, 10, 15, and 20 wt%, denoted as CNLDH-5, CNLDH-10, CNLDH-15, and CNLDH-20 by the authors, respectively) for realizing high-efficient photocatalytic  $CO_2$  reduction. The TEM images showed successful 2D/2D assembly and intimate interface of Ni-Al-LDH/g- $C_3N_4$  composite (Fig. 8a-c). The results of photocatalytic experiments showed that CNLDH-10 presented the highest activity to reduce  $CO_2$  to CO,  $H_2$ , and  $O_2$  (Fig. 8d, e, and f). The optimal evolution rate of CO with CNLDH-10 was reported to be 8.2  $\mu\text{mol/h/g}$ , and this value was much higher than that with only Ni-Al-LDH (0.92  $\mu\text{mol/h/g}$ ) and g- $C_3N_4$  (1.56  $\mu\text{mol/h/g}$ ). An experiment by using physical mixture of Ni-Al-LDH (10 wt%) and g- $C_3N_4$  as the

**Table 1**  
Constructing strategies and applications of some LDH/g- $C_3N_4$  binary photocatalysts.

Photocatalyst	Constructing strategy	Application	Reference
Mg-Al-LDH/g- $C_3N_4$	Electrostatic self-assembly	$CO_2$ reduction	[72]
Ni-Fe-LDH/g- $C_3N_4$	Electrostatic self-assembly	Water splitting	[73]
Zn-Cr-LDH/g- $C_3N_4$	Electrostatic self-assembly	Water splitting	[105]
Zn-Cr-LDH/modified g- $C_3N_4$	In-situ coprecipitation	Degradation of Congo red	[56]
Co-Mn-LDH/g- $C_3N_4$	In-situ coprecipitation	Water splitting	[78]
Zn-Al-LDH/g- $C_3N_4$	In-situ coprecipitation	Degradation of methylene blue	[79]
Ni-Al-LDH/g- $C_3N_4$	Hydrothermal method	$CO_2$ reduction	[53]
Co-Al-LDH/O-doped g- $C_3N_4$	Hydrothermal method	Degradation of methyl orange and bisphenol A	[54]
Ni-Ti-LDH/g- $C_3N_4$	Hydrothermal method	Degradation of amoxicillin	[55]
Zn-Cr-LDH/g- $C_3N_4$	Hydrothermal method	Water splitting	[83]
Ni-Ti-LDH/g- $C_3N_4$ film	Hydrothermal method	Degradation of methyl orange	[84]
Ni-Al-LDH/g- $C_3N_4$	Hydrothermal method	Degradation of rhodamine B and methyl orange	[106]
Zn-Al-LDH/g- $C_3N_4$	Solvothermal method	Degradation of methylene blue	[88]
Ni-Mn-LDH/g- $C_3N_4$	Solvothermal method	Degradation of rhodamine B	[91]
Co-Fe-LDH/g- $C_3N_4$	Solvothermal method	Water splitting	[92]

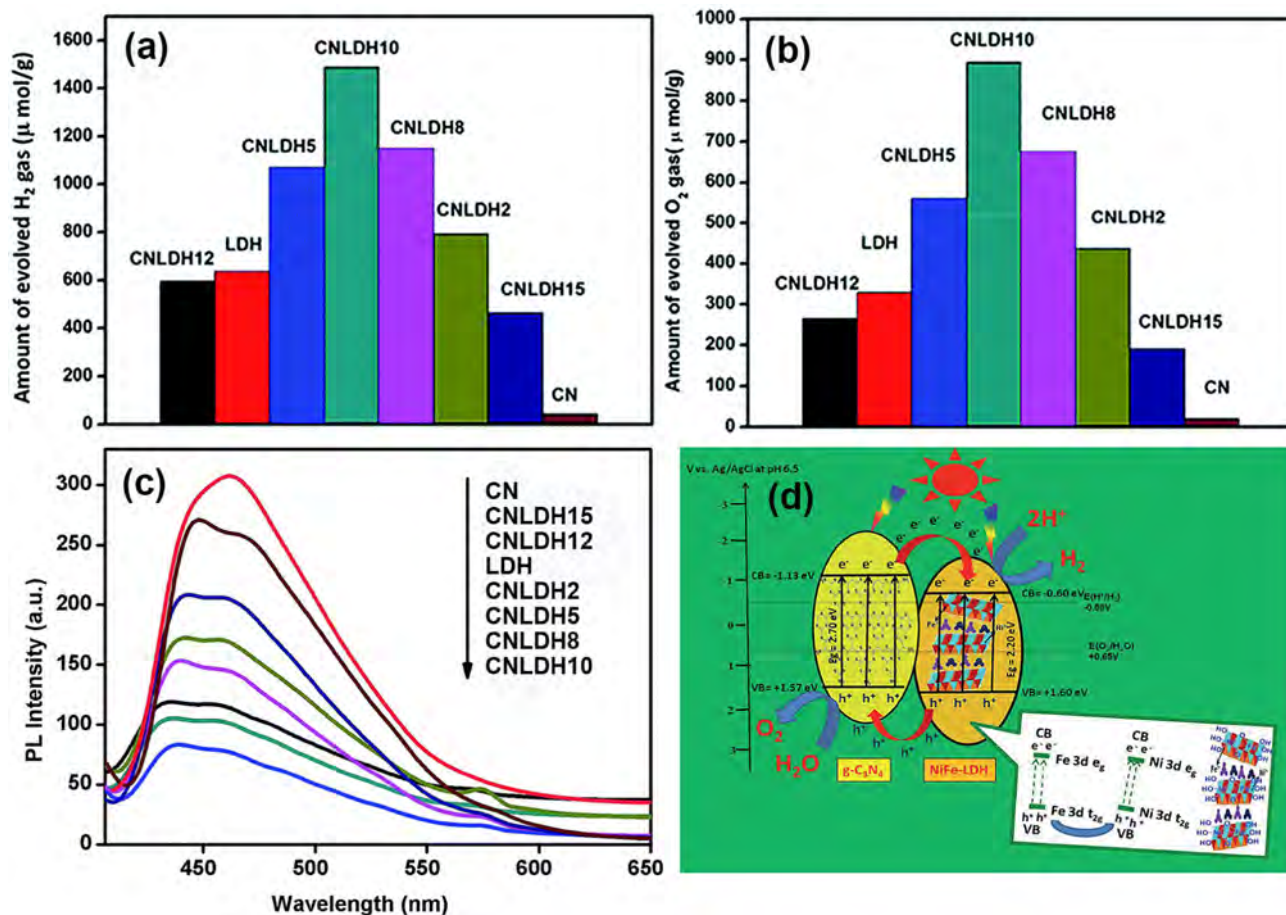
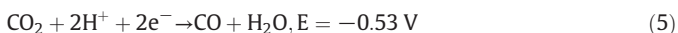
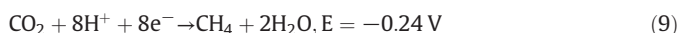
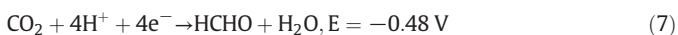
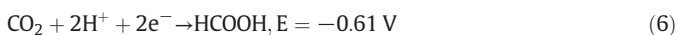


Fig. 7. (a) The amount of evolved hydrogen with Ni-Fe-LDH, g-C<sub>3</sub>N<sub>4</sub> and different Ni-Fe-LDH/g-C<sub>3</sub>N<sub>4</sub> composites in the photocatalytic water splitting; (b) the amount of evolved oxygen with Ni-Fe-LDH, g-C<sub>3</sub>N<sub>4</sub> and different Ni-Fe-LDH/g-C<sub>3</sub>N<sub>4</sub> composites in the photocatalytic water splitting; (c) photoluminescence spectra of Ni-Fe-LDH, g-C<sub>3</sub>N<sub>4</sub> and different Ni-Fe-LDH/g-C<sub>3</sub>N<sub>4</sub> composites; (d) proposed mechanism of the charge separation and transfer in Ni-Fe-LDH/g-C<sub>3</sub>N<sub>4</sub> composites for the evolution of hydrogen and oxygen under visible light irradiation. CN: g-C<sub>3</sub>N<sub>4</sub>, LDH: Ni-Fe-LDH, CNLDHn: Ni-Fe-LDH/g-C<sub>3</sub>N<sub>4</sub> containing n wt% g-C<sub>3</sub>N<sub>4</sub>. Reproduced with permission from ref. [73]. Copyright 2015 The Royal Society of Chemistry.

photocatalyst was carried out for comparison, and the evolution rate of CO was only 2.84 μmol/h/g. This result demonstrated the importance of intimate contact between LDH and g-C<sub>3</sub>N<sub>4</sub> in achieving high photocatalytic performance with LDH/g-C<sub>3</sub>N<sub>4</sub> composites. In the photocatalytic mechanism study, CNLDH-10 showed the lowest PL intensity and the highest transient photocurrent responses (Fig. 8g and h), which was consistent with its high photocatalytic performance in CO<sub>2</sub> reduction. The possible photocatalytic mechanism for CO<sub>2</sub> reduction by Ni-Al-LDH/g-C<sub>3</sub>N<sub>4</sub> photocatalyst was proposed and illustrated as shown in Fig. 8i. Both Ni-Al-LDH and g-C<sub>3</sub>N<sub>4</sub> could produce electrons and holes under the irradiation of visible light. The electrons on the CB of g-C<sub>3</sub>N<sub>4</sub> could transfer to the CB of Ni-Al-LDH, while the holes on the VB of Ni-Al-LDH could move to the VB of g-C<sub>3</sub>N<sub>4</sub>. The accumulated electrons on the CB of Ni-Al-LDH reduced CO<sub>2</sub> to CO. The reduction process of CO<sub>2</sub> was described by the following equation and redox potential (vs. NHE, at pH 7.00):



Except being reduced to CO for renewable fuels, CO<sub>2</sub> may also be reduced to HCOOH, HCHO, CH<sub>3</sub>OH, and CH<sub>4</sub> with different redox potential (vs. NHE, at pH 7.00) [107]:



For example, Hong et al. [72] constructed Mg-Al-LDH/g-C<sub>3</sub>N<sub>4</sub> photocatalysts and used them for reducing CO<sub>2</sub> to CH<sub>4</sub>. If this technique can be successfully applied in practical engineering, both the global warming and energy crisis will be alleviated.

Salehi et al. [106] synthesized Ni-Al-LDH/g-C<sub>3</sub>N<sub>4</sub> composites with various weight percentages of g-C<sub>3</sub>N<sub>4</sub> (10, 20, 30, 40, and 50 wt%, denoted as g-C<sub>3</sub>N<sub>4</sub>-10@NiAl-LDH, g-C<sub>3</sub>N<sub>4</sub>-20@NiAl-LDH, g-C<sub>3</sub>N<sub>4</sub>-30@NiAl-LDH, g-C<sub>3</sub>N<sub>4</sub>-40@NiAl-LDH, and g-C<sub>3</sub>N<sub>4</sub>-50@NiAl-LDH by the authors, respectively) and studied their photocatalytic activity for removing rhodamine B (RhB) and methyl orange (MO) in wastewater. Fig. 9a showed the typical 2D/2D structure of the synthesized Ni-Al-LDH/g-C<sub>3</sub>N<sub>4</sub> composites. The g-C<sub>3</sub>N<sub>4</sub>-40@NiAl-LDH displayed the highest photocatalytic performance in degrading RhB (Fig. 9b), while the g-C<sub>3</sub>N<sub>4</sub>-20@NiAl-LDH showed the highest photocatalytic performance in degrading MO (Fig. 9c). With the optimal photocatalyst, the removal rates of RhB and MO both reached 93% after visible light irradiation of 240 and 180 min, respectively. For elucidating the photocatalytic degradation mechanism, p-benzoquinone (BQ, ·O<sub>2</sub><sup>-</sup> scavenger), isopropanol (IPA, ·OH scavenger), and Na<sub>2</sub>-EDTA (h<sup>+</sup> scavenger) were used to identify important oxidative species in the Ni-Al-LDH/g-C<sub>3</sub>N<sub>4</sub> photocatalytic systems. The significant inhibition of dye degradation with the incorporation of isopropanol and Na<sub>2</sub>-EDTA implied that the generation of ·OH and h<sup>+</sup> mainly contributed to the dye degradation (Fig. 9d). As illustrated in Fig. 9e, ·OH could be generated when O<sub>2</sub> was reduced by the enriched electrons on the CB of Ni-Al-LDH. The



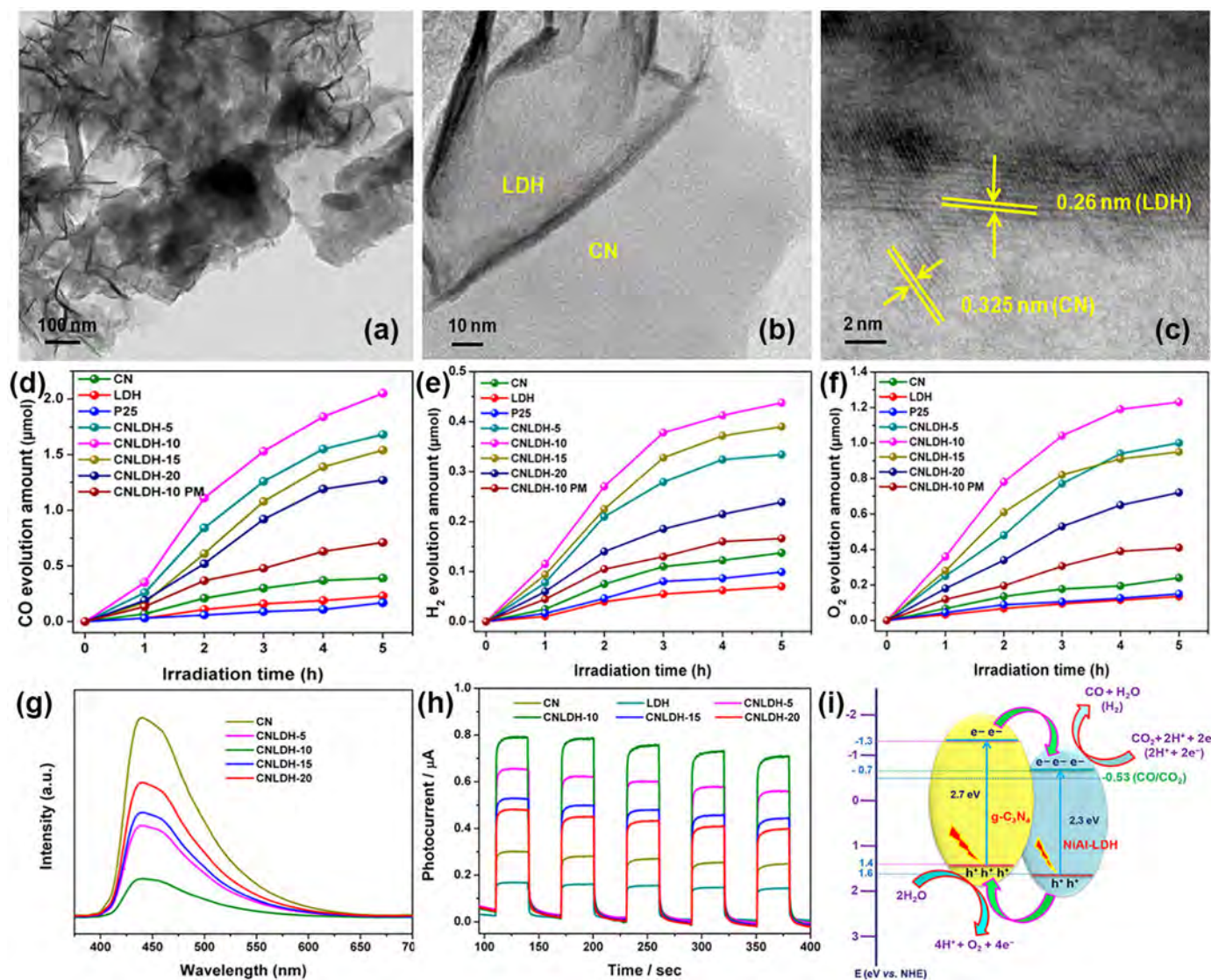
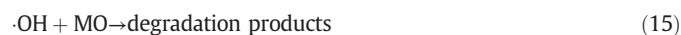


**Fig. 8.** (a and b) TEM images of CNLDH-10 composite; (c) high-resolution TEM image of CNLDH-10 composite; time-dependent evolution amount of (d) CO, (e) H<sub>2</sub>, and (f) O<sub>2</sub> over all the synthesized photocatalysts under visible light irradiation; (g) PL spectra of g-C<sub>3</sub>N<sub>4</sub>, Ni-Al-LDH, and Ni-Al-LDH/g-C<sub>3</sub>N<sub>4</sub>; (h) transient photocurrent responses of g-C<sub>3</sub>N<sub>4</sub>, Ni-Al-LDH, and Ni-Al-LDH/g-C<sub>3</sub>N<sub>4</sub>; (i) proposed mechanism for CO<sub>2</sub> photoreduction by the Ni-Al-LDH/g-C<sub>3</sub>N<sub>4</sub> photocatalyst. CN: g-C<sub>3</sub>N<sub>4</sub>, LDH: Ni-Al-LDH, CNLDH-n: Ni-Al-LDH/g-C<sub>3</sub>N<sub>4</sub> containing n wt% Ni-Al-LDH, P25: commercial P25 reference catalyst, CNLDH-10 PM: physical mixture of Ni-Al-LDH (10 wt%) and g-C<sub>3</sub>N<sub>4</sub>. Reproduced with permission from ref. [53]. Copyright 2018 American Chemical Society.

generated  $\cdot\text{OH}$  and accumulated  $\text{h}^+$  on the VB of g-C<sub>3</sub>N<sub>4</sub> contributed to the oxidative degradation of RhB and MO. Additionally,  $\text{h}^+$  could also lead to the formation of  $\cdot\text{OH}$ . Related reactions are expressed by the following equations:



In the experiments that assessed the photocatalytic performance of LDH/g-C<sub>3</sub>N<sub>4</sub> composites for removing organic pollutants, organic dyes were generally selected as model pollutants due to the relatively obvious experimental phenomenon and convenient measurement. Additionally, some antibiotics and endocrine disruptors were targeted in the degradation experiments [54,55]. Zhang et al. [88] fabricated Zn-Al-LDH/g-C<sub>3</sub>N<sub>4</sub> composites and applied them to degrade methylene blue (MB). In the experiments, Zn-Al-LDH/g-C<sub>3</sub>N<sub>4</sub> photocatalyst completely removed the MB under the irradiation of ultraviolet (UV) light for 60 min, while g-C<sub>3</sub>N<sub>4</sub> and Zn-Al-LDH could only remove 55.0% and 21.0% MB under the same conditions, respectively. This demonstrated the improved photocatalytic activity after the combination of Zn-Al-LDH and g-C<sub>3</sub>N<sub>4</sub>. However, commercial ZnO photocatalyst only took 20 min to completely remove the MB under UV light irradiation. Under the irradiation of visible light, the Zn-Al-LDH/g-C<sub>3</sub>N<sub>4</sub> photocatalyst removed 100% MB within 240 min, but only 27.2% MB was removed by the commercial ZnO photocatalyst under the same

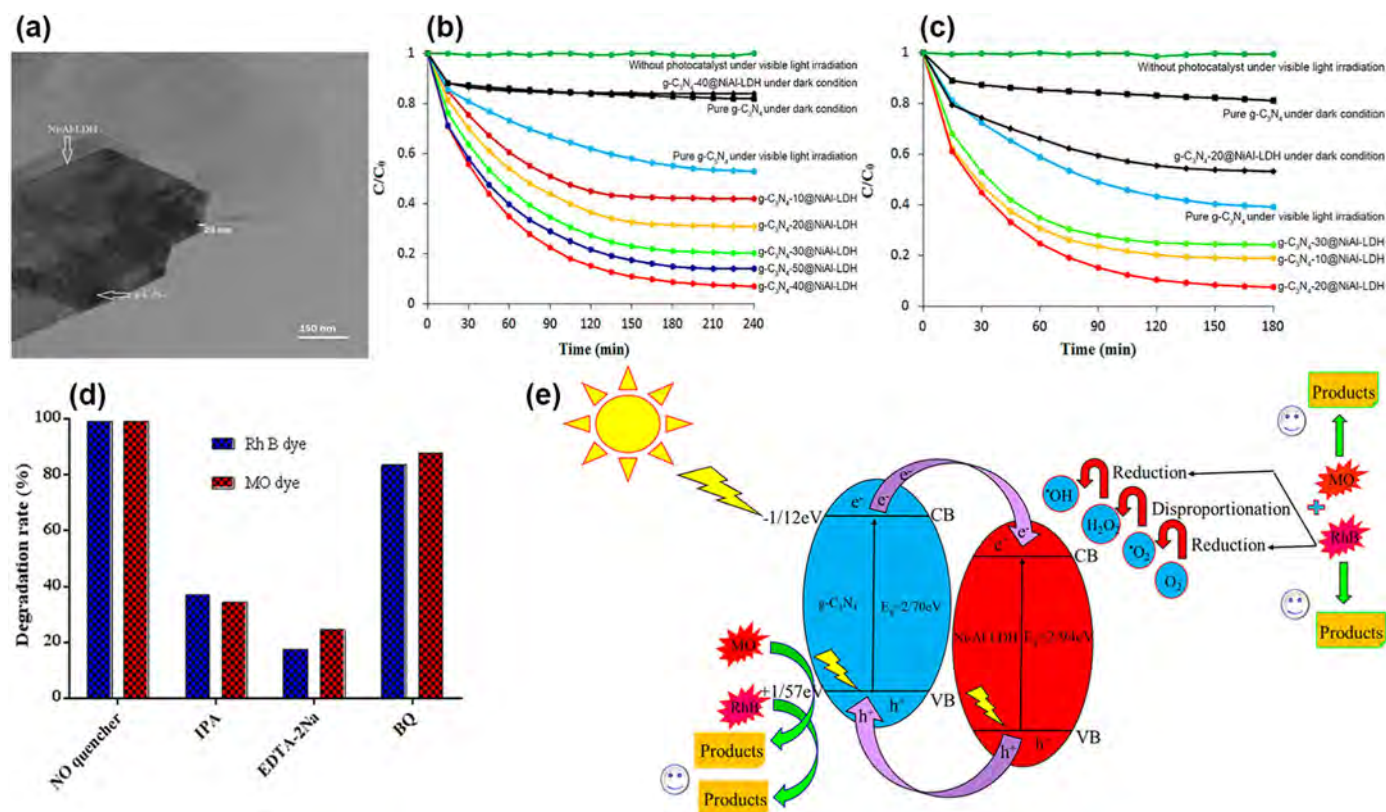


**Fig. 9.** (a) TEM image of the synthesized  $g\text{-C}_3\text{N}_4\text{-40@NiAl-LDH}$  composite; (b) photocatalytic activities for the degradation of rhodamine B under various conditions; (c) photocatalytic activities for the degradation of methyl orange under various conditions; (d) effects of various active scavengers on the degradation of rhodamine B by  $g\text{-C}_3\text{N}_4\text{-40@NiAl-LDH}$  and the degradation of methyl orange by  $g\text{-C}_3\text{N}_4\text{-20@NiAl-LDH}$  under visible light irradiation for 240 and 180 min, respectively; (e) possible mechanism for the photocatalytic degradation of rhodamine B and methyl orange by Ni-Al-LDH/ $g\text{-C}_3\text{N}_4$  composite under visible light irradiation.  $g\text{-C}_3\text{N}_4\text{-n@NiAl-LDH}$ : Ni-Al-LDH/ $g\text{-C}_3\text{N}_4$  composite containing n wt%  $g\text{-C}_3\text{N}_4$ , Rh B: rhodamine B, MO: methyl orange, IPA: isopropanol, BQ: p-benzoquinone. Reproduced with permission from ref. [106]. Copyright 2018 American Chemical Society.

conditions. The higher performance of Zn-Al-LDH/ $g\text{-C}_3\text{N}_4$  photocatalyst under visible light made it more competitive in solar photocatalysis. Considering the practical applications, Yazdani et al. [84] constructed Ni-Ti-LDH/ $g\text{-C}_3\text{N}_4$  films on quartz glass substrates and used them for photocatalytic degradation of MO. The films were placed in a reactor where the MO solution was circulated over the film surface under visible light irradiation. After a single run, the films could be directly taken out, washed, and dried for the next run. Immobilizing Ni-Ti-LDH/ $g\text{-C}_3\text{N}_4$  photocatalyst on the film simplified the process of recycling photocatalysts from aqueous solutions compared with using powder photocatalysts, which might be beneficial for the practical applications.

#### 4.2. LDH/ $g\text{-C}_3\text{N}_4$ /X ternary photocatalysts

Though coupling LDH and  $g\text{-C}_3\text{N}_4$  can increase the electron-hole separation, the charge carriers on some LDH/ $g\text{-C}_3\text{N}_4$  photocatalysts are difficult to further transfer and participate in redox reactions [108]. Therefore, constructing LDH/ $g\text{-C}_3\text{N}_4$ /X ternary photocatalysts is considered, where X represents other semiconductor or noble metal. This strategy is expected to not only facilitate the charge carrier transfer at the interface of LDH and  $g\text{-C}_3\text{N}_4$ , but also improve the harvesting ability for visible light. According to available literature, Ag and reduced graphene oxide (RGO) were primarily used to realize these goals [108–111].

Tonda and Jo [111] incorporated 1 wt% Ag nanoparticles into Ni-Al-LDH/ $g\text{-C}_3\text{N}_4$  composites with various weight percentages of Ni-Al-LDH (5, 10, 15, and 20 wt%, denoted as ALDHCN-5, ALDHCN-10, ALDHCN-15, and ALDHCN-20 by the authors, respectively) and studied their photocatalytic performance in degrading RhB and 4-chlorophenol (4-CP). In their study, the Ni-Al-LDH/ $g\text{-C}_3\text{N}_4$  composites were first fabricated through hydrothermal method, and then the composites

were decorated with Ag nanoparticles via a photo-reduction process to form Ni-Al-LDH/ $g\text{-C}_3\text{N}_4$ /Ag hybrids (Fig. 10a). The deposition of Ag nanoparticles on Ni-Al-LDH/ $g\text{-C}_3\text{N}_4$  was clearly observed with TEM image (Fig. 10b). The combination of Ni-Al-LDH and  $g\text{-C}_3\text{N}_4$  greatly increased the photocatalytic activity in degrading both RhB and 4-CP, while the incorporation of Ag nanoparticles further enhanced the photocatalytic performance (Fig. 10c and d). In the mechanism study, the photocatalytic activity of ALDHCN-15 was significantly inhibited in the presence of ammonium oxalate (AO,  $h^+$  scavenger), benzoquinone (BZQ,  $\cdot\text{O}_2^-$  scavenger), tert-butanol (TBA,  $\cdot\text{OH}$  scavenger). The order of inhibiting ability was BZQ > TBA > AO (Fig. 10e). This result demonstrated that  $\cdot\text{O}_2^-$  and  $\cdot\text{OH}$  were the main active species that accounted for the pollutant degradation. The generation of  $\cdot\text{OH}$  during the photocatalytic process was further confirmed by  $\cdot\text{OH}$  trapping PL spectra in terephthalic acid solution (Fig. 10f). The possible photocatalytic mechanism of Ni-Al-LDH/ $g\text{-C}_3\text{N}_4$ /Ag composite was illustrated in Fig. 10g. Both Ni-Al-LDH and  $g\text{-C}_3\text{N}_4$  could generate electron-hole pairs under visible light. Because the CB of  $g\text{-C}_3\text{N}_4$  ( $-1.32\text{eV}$ ) is more negative than that of Ni-Al-LDH ( $-0.72\text{eV}$ ), the electrons on the CB of  $g\text{-C}_3\text{N}_4$  could move to the CB of Ni-Al-LDH. Similarly, the holes on the VB of Ni-Al-LDH could transfer to the VB of  $g\text{-C}_3\text{N}_4$ . This facilitated the electron-hole separation. The surface Ag nanoparticles on the composites were excellent electron trappers, which could transfer electrons from the CB of both Ni-Al-LDH and  $g\text{-C}_3\text{N}_4$ . Therefore, the electron-hole separation efficiency was further enhanced, contributing to the higher photocatalytic performance. Nayak and Parida [109] added Ag@Ag<sub>3</sub>PO<sub>4</sub> component into Ni-Fe-LDH/ $g\text{-C}_3\text{N}_4$  to improve the performance for photocatalytic Cr(VI) reduction and phenol degradation. It was reported that Ag nanoparticles could induce surface plasmon resonance, in which free electrons on the surface of Ag nanoparticles oscillated collectively under the light irradiation. The plasmon resonance improved the light

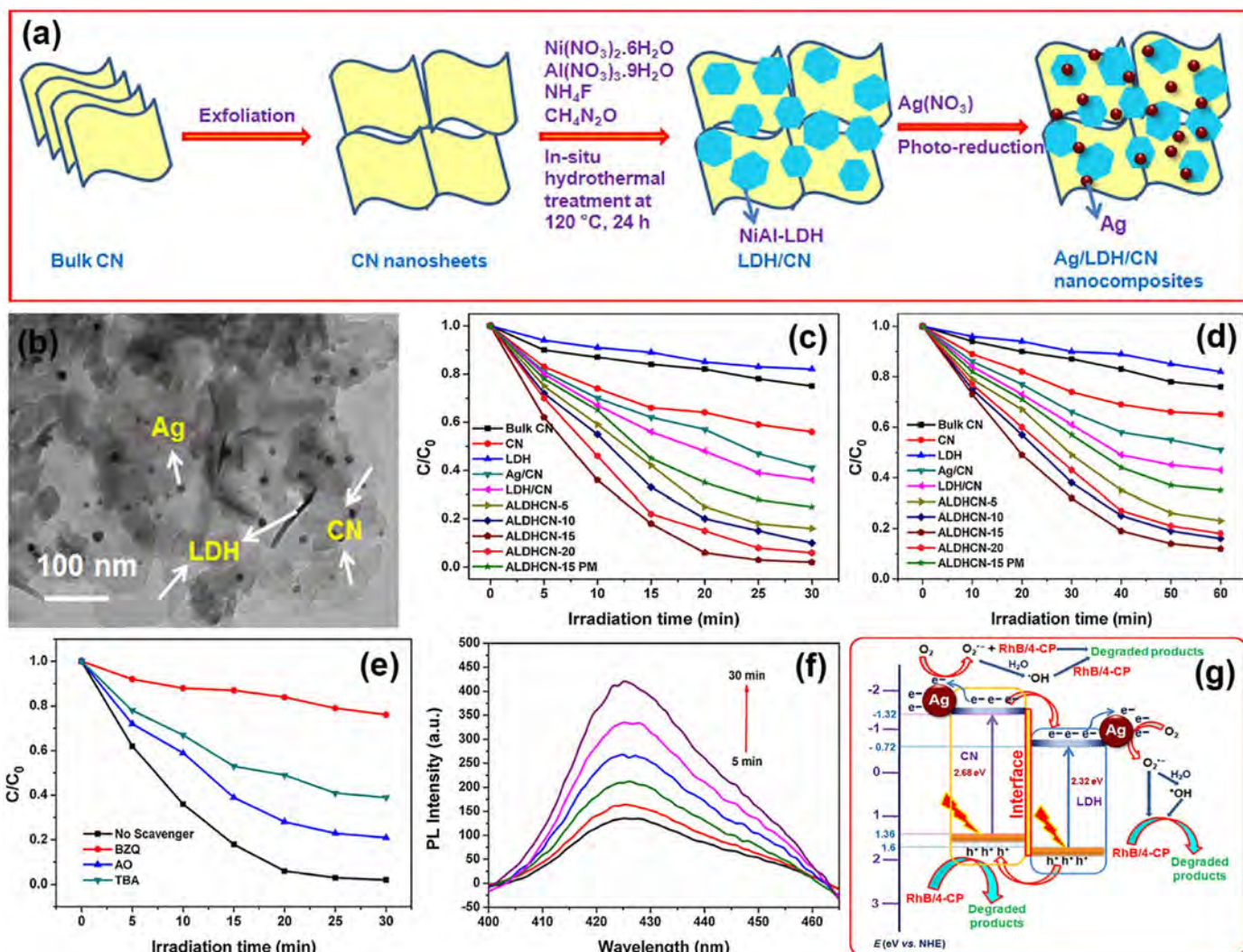


**Fig. 10.** (a) Schematic illustration of the synthesis of Ni-Al-LDH/g-C<sub>3</sub>N<sub>4</sub>/Ag face-to-face hybrid nanocomposites; (b) TEM images of the synthesized ALDHCN-15; (c) photocatalytic activities in the degradation of RhB over all the synthesized photocatalysts under visible light irradiation; (d) photocatalytic activities in the degradation of 4-CP over all the synthesized photocatalysts under visible light irradiation; (e) effects of different scavengers on the degradation of RhB with ALDHCN-15 under visible light irradiation; (f) ·OH trapping PL spectra of ALDHCN-15 in terephthalic acid solution under visible light irradiation; (g) schematic illustration of the charge separation and transfer in the Ni-Al-LDH/g-C<sub>3</sub>N<sub>4</sub>/Ag nanocomposite system under visible light irradiation. CN: g-C<sub>3</sub>N<sub>4</sub>, LDH: Ni-Al-LDH, ALDHCN-n: Ni-Al-LDH/g-C<sub>3</sub>N<sub>4</sub>/Ag containing n wt% Ni-Al-LDH, ALDHCN-15 PM: physical mixture of 15 wt% Ni-Al-LDH and CN (followed by 1 wt% Ag deposition), BZO: benzoquinone, AO: ammonium oxalate, TBA: tert-butanol. Reproduced with permission from ref. [111]. Copyright 2017 Elsevier.

harvesting capacity and thus enhanced the photocatalytic Cr(VI) reduction and phenol degradation. This offered another mechanism by which Ag nanoparticles promote the performance of LDH/g-C<sub>3</sub>N<sub>4</sub> photocatalyst.

Jo and Tonda [108] fabricated Co-Al-LDH/g-C<sub>3</sub>N<sub>4</sub>/RGO composites with 1 wt% RGO and various weight percentages of Co-Al-LDH (5, 10, 15, and 20 wt%, denoted as LCR-5, LCR-10, LCR-15, and LCR-20 by the authors, respectively) and applied them for photocatalytic degradation of Congo red (CR) and tetracycline (TC). The composites were synthesized by adding RGO suspension into the mixture of Co-Al-LDH and g-C<sub>3</sub>N<sub>4</sub> before the hydrothermal reaction (Fig. 11a). The TEM image of LCR-15 showed a typical 2D/2D/2D structure. The incorporation of RGO considerably improved the photocatalytic activity of Co-Al-LDH/g-C<sub>3</sub>N<sub>4</sub> composites in degrading CR and TC, and LCR-15 exhibited the highest photocatalytic performance for degrading both the pollutants. Due to the generation of intermediate products, the decoloration of CR is generally not equal to that the pollutant has been completely mineralized into CO<sub>2</sub> and H<sub>2</sub>O. Fig. 11e showed the removal of total organic carbon (TOC) by LCR-15 in removing CR, which suggested the pollutant

mineralization by the photocatalytic process. The LCR-15 photocatalyst could remove 79% TOC from CR solution under visible light for 30 min. The high photocatalytic activity of Co-Al-LDH/g-C<sub>3</sub>N<sub>4</sub>/RGO composites could be partly ascribed to the enhanced light harvesting ability due to the RGO incorporation. As shown in the UV-vis diffuse reflection spectra (DRS, Fig. 11f), the presence of RGO increased the absorption capacity of Co-Al-LDH/g-C<sub>3</sub>N<sub>4</sub>/RGO for visible light. Additionally, because of the conductivity of RGO, the generated electrons on the CB of both Co-Al-LDH and g-C<sub>3</sub>N<sub>4</sub> could transfer along the RGO network, further enhancing the electron-hole separation for degrading CR and TC (Fig. 11g). Nayak and Parida [110] added N-doped RGO into Ni-Fe-LDH/g-C<sub>3</sub>N<sub>4</sub> to increase the photocatalytic activity in degrading RhB and phenol, as well as producing H<sub>2</sub> and O<sub>2</sub>. Doping nitrogen on the RGO networks facilitated the charge transfer between adjacent carbon atoms. The direct coupling of N-doped RGO and transition-metal atom sites on Ni-Fe-LDH accelerated the charge transfer at the interface of LDH/g-C<sub>3</sub>N<sub>4</sub>. These attempts provided valuable experience for using RGO to further promote charge transfer at the interface of LDH/g-C<sub>3</sub>N<sub>4</sub> and the absorption capacity for visible light.

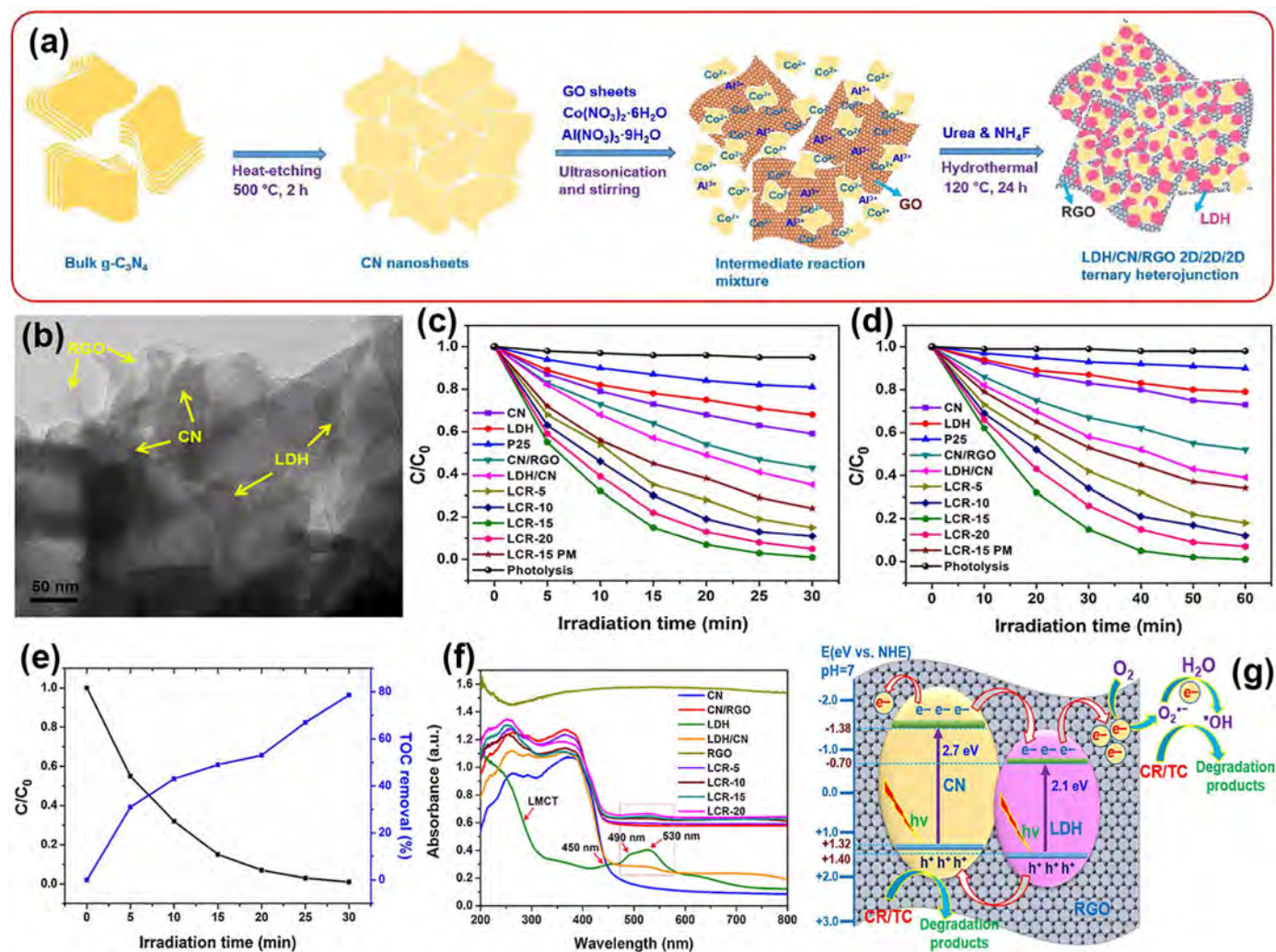


**Fig. 11.** (a) Schematic representation of the fabrication of Co-Al-LDH/g-C<sub>3</sub>N<sub>4</sub>/RGO 2D/2D/2D ternary heterojunction; (b) TEM image of LCR-15 photocatalyst; (c) the photocatalytic activities over all the fabricated catalysts in the degradation of CR; (d) the photocatalytic activities over all the fabricated catalysts in the degradation of TC; (e) comparison of the photocatalytic performance and TOC removal over the LCR-15 photocatalyst in the degradation of CR; (f) UV-vis DRS patterns of all the fabricated samples; (g) schematic diagram illustrating the photocatalytic mechanism for the degradation of CR and TC over the Co-Al-LDH/g-C<sub>3</sub>N<sub>4</sub>/RGO ternary heterojunction system. CN: g-C<sub>3</sub>N<sub>4</sub>, LDH: Co-Al-LDH, LCR-n: Co-Al-LDH/g-C<sub>3</sub>N<sub>4</sub>/RGO containing n wt% Co-Al-LDH, P25: commercial P25 reference catalyst, LCR-15 PM: physical mixture of 15 wt% Co-Al-LDH, 1 wt% RGO and g-C<sub>3</sub>N<sub>4</sub>. Reproduced with permission from ref. [108]. Copyright 2019 Elsevier.

#### 4.3. Calcined LDH/g-C<sub>3</sub>N<sub>4</sub> photocatalysts

Calcining LDH/g-C<sub>3</sub>N<sub>4</sub> composites or using LDHs as precursors can fabricate calcined LDH/g-C<sub>3</sub>N<sub>4</sub> with higher surface area and better photocatalytic activity [60,94,96–100]. The topological transformation of homogeneous LDHs ensures the formation of highly dispersed MMOs on g-C<sub>3</sub>N<sub>4</sub>. Besides metal oxides, the calcination of LDHs may generate spinels which present smaller band gap than metal oxides and can serve as light sensitizer to increase the harvesting ability for visible light [96,97].

Lan et al. [100] fabricated some calcined Zn-In-LDH/g-C<sub>3</sub>N<sub>4</sub> composites from different weight ratios of melamine and Zn-In-LDH (1:1, 3:1, and 5:1, denoted as 1-MMO/C<sub>3</sub>N<sub>4</sub>, 3-MMO/C<sub>3</sub>N<sub>4</sub>, and 5-MMO/C<sub>3</sub>N<sub>4</sub> by the authors, respectively). These composites were applied for the degradation of RhB. Fig. 12a showed the 2D layered structure of the calcined Zn-In-LDH/g-C<sub>3</sub>N<sub>4</sub> composite. The XRD patterns suggested that ZnO had a higher crystallinity than In<sub>2</sub>O<sub>3</sub> in the calcined Zn-In-LDH/g-C<sub>3</sub>N<sub>4</sub> composites (Fig. 12b). The 3-MMO/C<sub>3</sub>N<sub>4</sub> showed the highest photocatalytic activity for RhB degradation, showing a complete removal of RhB within 60 min (Fig. 12c). Additionally, the degradation efficiency of RhB was still over 95% after the 3-MMO/C<sub>3</sub>N<sub>4</sub> was recycled for eight times,

which indicated the stability of photocatalyst (Fig. 12d). The higher photocatalytic performance of calcined Zn-In-LDH/g-C<sub>3</sub>N<sub>4</sub> composite was attributed to higher photocurrent response (Fig. 12e), and the generation of more ·O<sub>2</sub><sup>-</sup> and ·OH (Fig. 12f and g). The possible mechanism for the carrier transfer was illustrated in Fig. 12h. Under visible light irradiation, many charge carriers were generated on the g-C<sub>3</sub>N<sub>4</sub> and In<sub>2</sub>O<sub>3</sub>. The transfer of electrons and holes through the heterojunction interface separated the charge carriers and enriched holes on the VB of g-C<sub>3</sub>N<sub>4</sub> and electrons on the CB of In<sub>2</sub>O<sub>3</sub>. The ZnO further improved the charge separation efficiency because of the excellent electron mobility of ZnO. The electrons could be accepted by oxygen to generate ·O<sub>2</sub><sup>-</sup> and ·OH, and these strong oxidants decomposed the RhB. Shi et al. [60] constructed 2D/2D calcined Mg-Fe-LDH/g-C<sub>3</sub>N<sub>4</sub> photocatalyst and achieved an improved H<sub>2</sub> production under the irradiation of visible light. In their experiments, it was found that the CB position was tunable and the product with a smaller CB potential could be obtained with a more addition amount of calcined Mg-Fe-LDH. The result provided valuable information for tuning band structure of LDH/g-C<sub>3</sub>N<sub>4</sub> photocatalyst to meet the demands in different applications.

Di et al. [97] synthesized several kinds of calcined Zn-Fe-LDH/g-C<sub>3</sub>N<sub>4</sub> composites with various weight percentages of g-C<sub>3</sub>N<sub>4</sub> (0.5, 1.0, 5.0, 70,

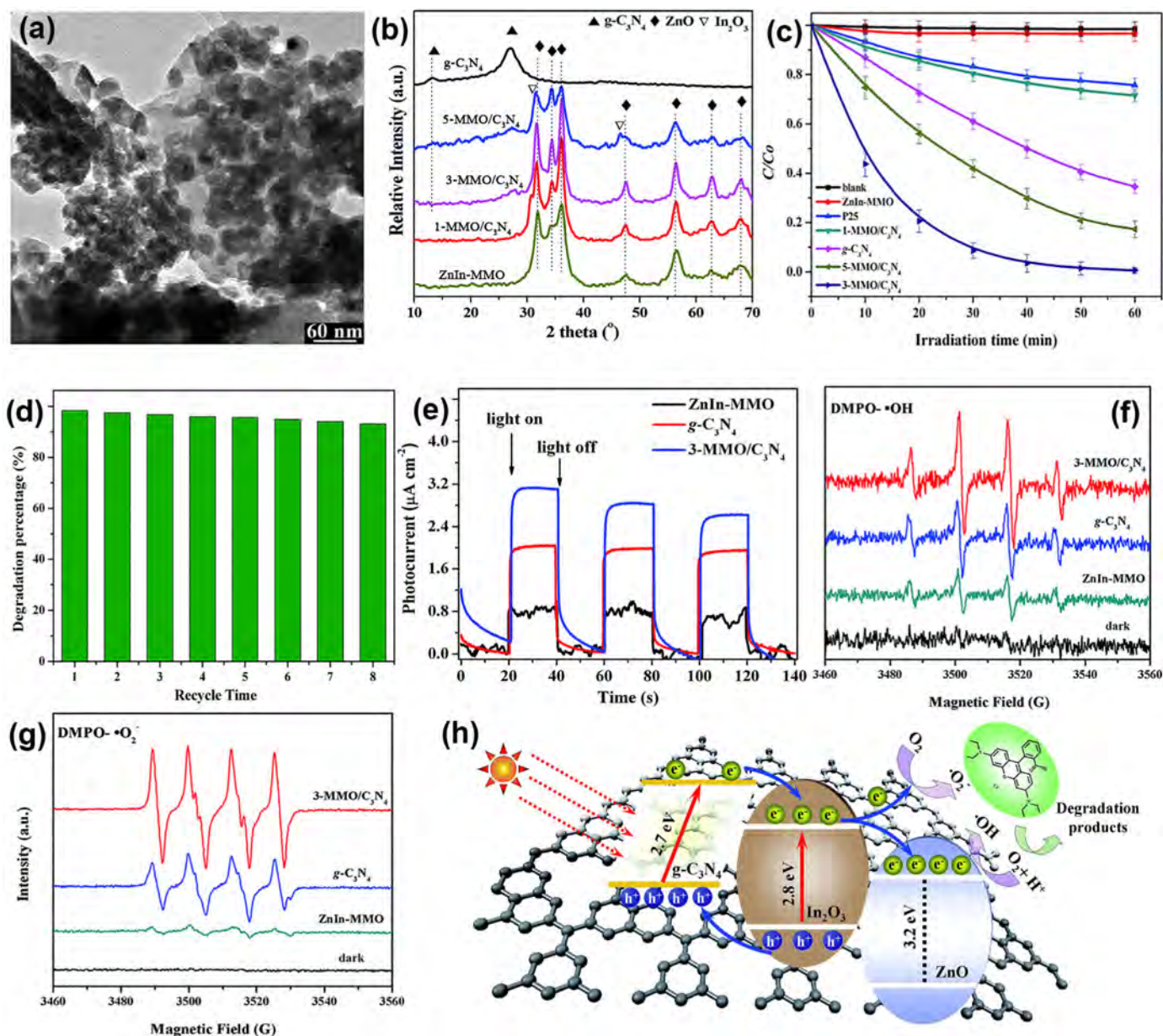


**Fig. 12.** (a) TEM image of 3-MMO/C<sub>3</sub>N<sub>4</sub>; (b) XRD patterns of all the prepared photocatalyst; (c) photocatalytic degradation of RhB over different photocatalysts under visible light irradiation; (d) cycling runs of 3-MMO/C<sub>3</sub>N<sub>4</sub> in the photodegradation of RhB; (e) photocurrent profiles of ZnIn-MMO, g-C<sub>3</sub>N<sub>4</sub> and 3-MMO/C<sub>3</sub>N<sub>4</sub>; (f) DMPO spin-trapping ESR spectra for DMPO-·OH in aqueous solution; (g) DMPO spin-trapping ESR spectra for DMPO-·O<sub>2</sub> in dimethyl sulfoxide (DMSO); (h) proposed mechanism of charge separation and photocatalytic activity over ZnIn-MMO/g-C<sub>3</sub>N<sub>4</sub> photocatalyst under visible light irradiation. Reproduced with permission from ref. [100]. Copyright 2015 The Royal Society of Chemistry.

and 90, denoted as CNZF-0.5, CNZF-1.0, CNZF-5.0, CNZF-70, and CNZF-90 by the authors, respectively) and explored their photocatalytic activity in degrading ibuprofen (IBF) and sulfadiazine (SDZ). The high-resolution TEM images showed the intimate face-to-face contact between calcined Zn-Fe-LDH and g-C<sub>3</sub>N<sub>4</sub> (Fig. 13a and b). The characteristic diffractions of ZnO and ZnFe<sub>2</sub>O<sub>4</sub> were observed with the XRD pattern of calcined Zn-Fe-LDH (Fig. 13c). The CNZF-1.0 and CNZF-90 exhibited the best photocatalytic performance among the prepared photocatalysts in the IBF and SDZ degradation process, respectively (Fig. 13d and e). Different scavengers for h<sup>+</sup> (Na<sub>2</sub>-EDTA), ·O<sub>2</sub> (BQ), and ·OH (IPA) were used in the photocatalytic systems to identify the main oxidative species that accounted for the pollutant degradation. It was found that h<sup>+</sup> mainly contributed to the degradation of IBF by CNZF-1.0 photocatalyst (Fig. 13f), and the degradation of SDZ by CNZF-90 mainly resulted from the generation of ·OH (Fig. 13g). A Z-scheme charge transfer mechanism was proposed for explaining the

improved photocatalytic performance of calcined Zn-Fe-LDH/g-C<sub>3</sub>N<sub>4</sub> composites (Fig. 13h). The authors did not directly present the inference process about the Z-scheme charge transfer mechanism. However, it was indicated by their experimental results. The photoinduced generation of ·OH on Zn-Fe-LDH/g-C<sub>3</sub>N<sub>4</sub> was ascertained by electron paramagnetic resonance (EPR) spectra (Fig. 13h). The redox potential needed for ·OH generation was more positive than the VB potential of g-C<sub>3</sub>N<sub>4</sub>. If the photoinduced h<sup>+</sup> accumulated on VB of g-C<sub>3</sub>N<sub>4</sub>, the resulting redox ability would be insufficient for ·OH generation [112]. Therefore, it should be a Z-scheme charge transfer mechanism. Under visible light irradiation, both g-C<sub>3</sub>N<sub>4</sub> and ZnO in the heterojunction could generate electron-hole pairs. The generated electrons on the CB of ZnO could move to the VB of g-C<sub>3</sub>N<sub>4</sub> and recombine with the holes generated there. This resulted in the electron-hole separation, and the accumulation of electrons on the CB of g-C<sub>3</sub>N<sub>4</sub> and holes on the VB of ZnO contributed to the removal of IBF and SDZ. The ZnFe<sub>2</sub>O<sub>4</sub> spinel phase played a

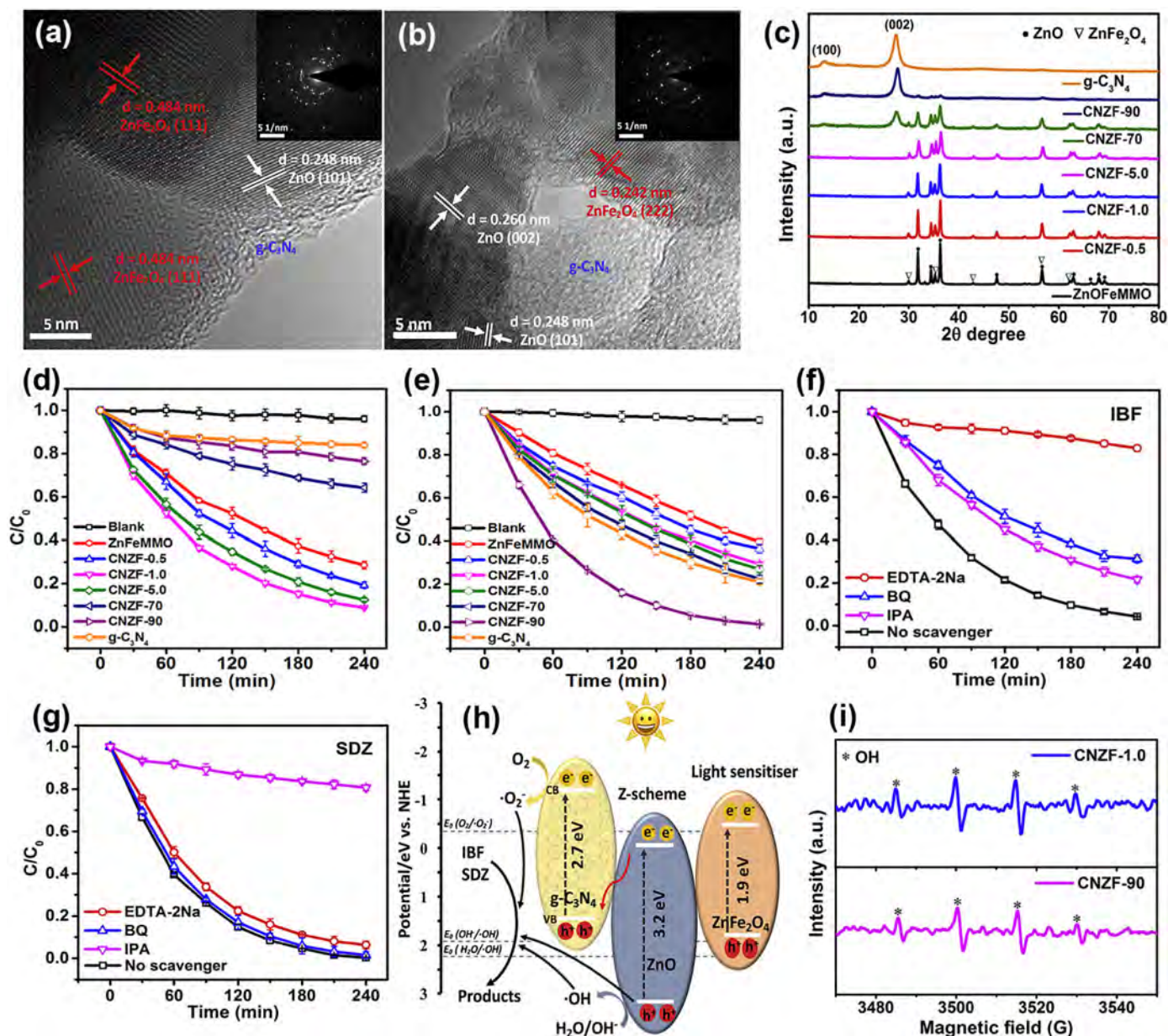


**Fig. 13.** (a–b) High-resolution TEM images and corresponding selected area electron diffraction (SAED) patterns of CNZF-1.0 and CNZF-90; (c) XRD patterns for all the prepared composites; (d) photodegradation of IBF over as-prepared photocatalysts under simulated solar irradiation; (e) photodegradation of SDZ over as-prepared photocatalysts under simulated solar irradiation; (f) IBF photodegradation over CNZF-1.0 in the presence of 1.0 mM various scavengers; (g) SDZ photodegradation over CNZF-90 in the presence of 1.0 mM various scavengers; (h) schematic illustration for the charge-transfer and photocatalytic mechanisms of calcined Zn-Fe-LDH/g-C<sub>3</sub>N<sub>4</sub> composites. (i) EPR spectra of DMPO·OH over CNZF-1.0 and CNZF-90 upon irradiation for 5 min. ZnFeMMO: calcined Zn-Fe-LDH, CNZF-n: calcined Zn-Fe-LDH/g-C<sub>3</sub>N<sub>4</sub> composites with n wt% of g-C<sub>3</sub>N<sub>4</sub>. Reproduced with permission from ref. [97]. Copyright 2018 Elsevier.

role of light sensitizer, which enhanced the light harvesting and charge carrier generation. Similar role of ZnCr<sub>2</sub>O<sub>4</sub> spinel phase in the calcined Zn-Cr-LDH/g-C<sub>3</sub>N<sub>4</sub> photocatalyst was reported by Patnaik et al. [96]. Because of smaller band gap of ZnCr<sub>2</sub>O<sub>4</sub> (1.5 eV) than that of ZnO (3.2 eV), ZnCr<sub>2</sub>O<sub>4</sub> could harvest visible light and sensitize ZnO to promote the photocatalytic performance. These studies suggested that the formation of spinel phase in calcined LDH/g-C<sub>3</sub>N<sub>4</sub> could increase photocatalytic performance by enhancing the absorption of visible light.

## 5. Conclusion and outlook

In summary, constructing 2D/2D LDH/g-C<sub>3</sub>N<sub>4</sub> heterojunction is an effective approach to achieve high performance in solar photocatalysis for pollution abatement and energy conversion. The planar structure and face-to-face contact of LDH and g-C<sub>3</sub>N<sub>4</sub> can greatly facilitate the

separation and transfer of photoinduced charge carriers, thus improving the photocatalytic performance. Many synthesis methods including electrostatic self-assembly, in-situ coprecipitation, hydrothermal method, solvothermal method, and calcination method have been developed for constructing LDH/g-C<sub>3</sub>N<sub>4</sub> heterojunction with desired 2D/2D structure and rational band gaps. The synergetic effect of LDH and g-C<sub>3</sub>N<sub>4</sub> has contributed to high photocatalytic performance in hydrogen production, CO<sub>2</sub> reduction, and organic pollutant degradation. Fabricating LDH/g-C<sub>3</sub>N<sub>4</sub>/X ternary photocatalysts and calcined LDH/g-C<sub>3</sub>N<sub>4</sub> composites is effective for further improving and optimizing the photocatalytic performance. The following points may be considered in future research:

- (1) Increasing the harvesting ability for visible light and even near infrared light that accounts for >50% of solar irradiation. Though

LDH/g-C<sub>3</sub>N<sub>4</sub> photocatalysts can function under visible light, the harvesting ability for sun light may be further improved through surface sensitization, doping element, band gap adjustment, etc.

- (2) Matching the CB (or VB) potential of LDH/g-C<sub>3</sub>N<sub>4</sub> photocatalysts with the redox potential for specific photocatalytic reaction. Since the band structure of LDH/g-C<sub>3</sub>N<sub>4</sub> is tunable, it is possible to adjust the CB (or VB) position to provide high redox potential for various photocatalytic reactions. However, the accurate adjustment method needs further study.
- (3) Going deep into the transfer mechanism of charge carriers. Better understanding of the mechanism is helpful for seeking more LDH materials that can combine with g-C<sub>3</sub>N<sub>4</sub> to achieve better photocatalytic performance.
- (4) Photocatalytic reaction mechanisms. How the reactants contact and interact with the LDH/g-C<sub>3</sub>N<sub>4</sub> photocatalysts, and the effects of photocatalyst properties (e.g., size and porosity) on the photocatalytic activity need to be further illuminated.
- (5) Constructing ultrathin 2D/2D structure. Some studies have proposed the ultrathin LDH and g-C<sub>3</sub>N<sub>4</sub> as photocatalysts [113–115]. It is also possible to construct ultrathin LDH/g-C<sub>3</sub>N<sub>4</sub> heterostructure that will enable faster carrier transfer due to the further shortened transfer distance from inner to surface and reduced electron-hole recombination in the bulk phase.
- (6) Application expansion. Current uses of LDH/g-C<sub>3</sub>N<sub>4</sub> composites mainly target at photocatalytic water splitting and organic pollutant degradation. The application for CO<sub>2</sub> reduction is relatively fewer. Existing and new LDH/g-C<sub>3</sub>N<sub>4</sub> photocatalysts may also be explored for applications in degradation of other more organic pollutants, Cr(VI) reduction, and nitrogen fixation. Simultaneously, the photocatalytic conditions should be recorded and optimized in different applications.
- (7) Practical engineering applications. Most studies were conducted under laboratory conditions. Considering the practical applications, the design of applicable reaction systems for LDH/g-C<sub>3</sub>N<sub>4</sub> photocatalysts is required.

## Declaration of Competing Interest

None

## Acknowledgements

This work was supported by National Natural Science Foundation of China (51378190, 51508177, 51521006, 51579095, 51709101), the Program for Changjiang Scholars and Innovative Research Team in University (IRT-13R17).

## References

- [1] Song B, Zeng G, Gong J, Liang J, Xu P, Liu Z, et al. Evaluation methods for assessing effectiveness of in situ remediation of soil and sediment contaminated with organic pollutants and heavy metals. *Environ Int* 2017;105:43–55.
- [2] Gong JL, Wang B, Zeng GM, Yang CP, Niu CG, Niu QY, et al. Removal of cationic dyes from aqueous solution using magnetic multi-wall carbon nanotube nanocomposite as adsorbent. *J Hazard Mater* 2009;164:1517–22.
- [3] Tang X, Zeng G, Fan C, Zhou M, Tang L, Zhu J, et al. Chromosomal expression of CadR on *Pseudomonas aeruginosa* for the removal of Cd(II) from aqueous solutions. *Sci Total Environ* 2018;636:1355–61.
- [4] Ye S, Zeng G, Wu H, Zhang C, Liang J, Dai J, et al. Co-occurrence and interactions of pollutants, and their impacts on soil remediation—a review. *Crit Rev Environ Sci Technol* 2017;47:1528–53.
- [5] Song B, Chen M, Ye S, Xu P, Zeng G, Gong J, et al. Effects of multi-walled carbon nanotubes on metabolic function of the microbial community in riverine sediment contaminated with phenanthrene. *Carbon* 2019;144:1–7.
- [6] Jiang D, Chen M, Wang H, Zeng G, Huang D, Cheng M, et al. The application of different typological and structural MOFs-based materials for the dyes adsorption. *Coord Chem Rev* 2019;380:471–83.
- [7] Kabir E, Kumar P, Kumar S, Adelodun AA, Kim K-H. Solar energy: potential and future prospects. *Renew Sust Energy Rev* 2018;82:894–900.
- [8] Borges ME, Sierra M, Cuevas E, García RD, Esparza P. Photocatalysis with solar energy: sunlight-responsive photocatalyst based on TiO<sub>2</sub> loaded on a natural material for wastewater treatment. *Sol Energy* 2016;135:527–35.
- [9] Spasiano D, Marotta R, Malato S, Fernandez-Ibañez P, Di Somma I. Solar photocatalysis: materials, reactors, some commercial, and pre-industrialized applications. A comprehensive approach. *Appl Catal B Environ* 2015;170–171:90–123.
- [10] Yang Y, Zhang C, Lai C, Zeng G, Huang D, Cheng M, et al. BiOX (X = Cl, Br, I) photocatalytic nanomaterials: applications for fuels and environmental management. *Adv Colloid Interf Sci* 2018;254:76–93.
- [11] Lai C, Zhang M, Li B, Huang D, Zeng G, Qin L, et al. Fabrication of CuS/BiVO<sub>4</sub> (0 4 0) binary heterojunction photocatalysts with enhanced photocatalytic activity for Ciprofloxacin degradation and mechanism insight. *Chem Eng J* 2019;358:891–902.
- [12] Li B, Lai C, Zeng G, Qin L, Yi H, Huang D, et al. Facile hydrothermal synthesis of Z-scheme Bi<sub>2</sub>Fe<sub>4</sub>O<sub>9</sub>/Bi<sub>2</sub>WO<sub>6</sub> heterojunction photocatalyst with enhanced visible light photocatalytic activity. *ACS Appl Mater Interfaces* 2018;10:18824–36.
- [13] Zhou C, Lai C, Huang D, Zeng G, Zhang C, Cheng M, et al. Highly porous carbon nitride by supramolecular preassembly of monomers for photocatalytic removal of sulfamethazine under visible light driven. *Appl Catal B Environ* 2018;220:202–10.
- [14] He K, Chen G, Zeng G, Chen A, Huang Z, Shi J, et al. Three-dimensional graphene supported catalysts for organic dyes degradation. *Appl Catal B Environ* 2018;228:19–28.
- [15] Yang D, Zhao X, Zou X, Zhou Z, Jiang Z. Removing Cr (VI) in water via visible-light photocatalytic reduction over Cr-doped SrTiO<sub>3</sub> nanoplates. *Chemosphere* 2019;215:586–95.
- [16] Kretschmer I, Senn AM, Meichtry JM, Custo G, Halac EB, Dillert R, et al. Photocatalytic reduction of Cr(VI) on hematite nanoparticles in the presence of oxalate and citrate. *Appl Catal B Environ* 2019;242:218–26.
- [17] Wang T, Sun M, Sun H, Shang J, Wong PK. Efficient Z-scheme visible-light-driven photocatalytic bacterial inactivation by hierarchical MoS<sub>2</sub>-encapsulated hydrothermal carbonation carbon core-shell nanospheres. *Appl Surf Sci* 2019;464:43–52.
- [18] Wang W, Li G, An T, Chan DKL, Yu JC, Wong PK. Photocatalytic hydrogen evolution and bacterial inactivation utilizing sonochemical-synthesized g-C<sub>3</sub>N<sub>4</sub>/red phosphorus hybrid nanosheets as a wide-spectral-responsive photocatalyst: the role of type I band alignment. *Appl Catal B Environ* 2018;238:126–35.
- [19] Kandy MM, Gaikar VG. Enhanced photocatalytic reduction of CO<sub>2</sub> using CdS/Mn<sub>2</sub>O<sub>3</sub> nanocomposite photocatalysts on porous anodic alumina support with solar concentrators. *Renew Energy* 2019;139:915–23.
- [20] Yang X, Hu Z, Yin Q, Shu C, Jiang XF, Zhang J, et al. Water-soluble conjugated molecule for solar-driven hydrogen evolution from salt water. *Adv Funct Mater* 2019;29:1808156.
- [21] Dong J, Shi Y, Huang C, Wu Q, Zeng T, Yao W. A new and stable Mo-Mo<sub>2</sub>C modified g-C<sub>3</sub>N<sub>4</sub> photocatalyst for efficient visible light photocatalytic H<sub>2</sub> production. *Appl Catal B Environ* 2019;243:27–35.
- [22] Tahir M. Hierarchical 3D VO<sub>2</sub>/ZnV<sub>2</sub>O<sub>4</sub> microspheres as an excellent visible light photocatalyst for CO<sub>2</sub> reduction to solar fuels. *Appl Surf Sci* 2019;467–468:1170–80.
- [23] Yang Y, Zeng Z, Zhang C, Huang D, Zeng G, Xiao R, et al. Construction of iodine vacancy-rich BiOI/Ag@AgI Z-scheme heterojunction photocatalysts for visible-light-driven tetracycline degradation: transformation pathways and mechanism insight. *Chem Eng J* 2018;349:808–21.
- [24] Zhou C, Lai C, Zhang C, Zeng G, Huang D, Cheng M, et al. Semiconductor/boron nitride composites: synthesis, properties, and photocatalysis applications. *Appl Catal B Environ* 2018;238:6–18.
- [25] Ye S, Yan M, Tan X, Liang J, Zeng G, Wu H, et al. Facile assembled biochar-based nanocomposite with improved graphitization for efficient photocatalytic activity driven by visible light. *Appl Catal B Environ* 2019;250:78–88.
- [26] Yi H, Yan M, Huang D, Zeng G, Lai C, Li M, et al. Synergistic effect of artificial enzyme and 2D nano-structured Bi<sub>2</sub>WO<sub>6</sub> for eco-friendly and efficient biomimetic photocatalysis. *Appl Catal B Environ* 2019;250:52–62.
- [27] Ong WJ, Tan LL, Ng YH, Yong ST, Chai SP. Graphitic carbon nitride (g-C<sub>3</sub>N<sub>4</sub>)-based photocatalysts for artificial photosynthesis and environmental remediation: are we a step closer to achieving sustainability? *Chem Rev* 2016;116:7159–329.
- [28] Kumar S, Karthikeyan S, Lee AF. g-C<sub>3</sub>N<sub>4</sub>-based nanomaterials for visible light-driven photocatalysis. *Catalysts* 2018;8:74.
- [29] Wang X, Maeda K, Thomas A, Takanabe K, Xin G, Carlsson JM, et al. A metal-free polymeric photocatalyst for hydrogen production from water under visible light. *Nat Mater* 2009;8:76–80.
- [30] Wen J, Xie J, Chen X, Li X. A review on g-C<sub>3</sub>N<sub>4</sub>-based photocatalysts. *Appl Surf Sci* 2017;391:72–123.
- [31] Fu J, Yu J, Jiang C, Cheng B. g-C<sub>3</sub>N<sub>4</sub>-based heterostructured photocatalysts. *Adv Energy Mater* 2018;8:1701503.
- [32] Xiong T, Cen W, Zhang Y, Dong F. Bridging the g-C<sub>3</sub>N<sub>4</sub> interlayers for enhanced photocatalysis. *ACS Catal* 2016;6:2462–72.
- [33] Mamba G, Mishra AK. Graphitic carbon nitride (g-C<sub>3</sub>N<sub>4</sub>) nanocomposites: a new and exciting generation of visible light driven photocatalysts for environmental pollution remediation. *Appl Catal B Environ* 2016;198:347–77.
- [34] Xie L, Ai Z, Zhang M, Sun R, Zhao W. Enhanced hydrogen evolution in the presence of plasmonic Au-photo-sensitized g-C<sub>3</sub>N<sub>4</sub> with an extended absorption spectrum from 460 to 640 nm. *PLoS One* 2016;11:e0161397.
- [35] Li X, Pi Y, Wu L, Xia Q, Wu J, Li Z, et al. Facilitation of the visible light-induced Fenton-like excitation of H<sub>2</sub>O<sub>2</sub> via heterojunction of g-C<sub>3</sub>N<sub>4</sub>/NH<sub>2</sub>-iron terephthalate metal-organic framework for MB degradation. *Appl Catal B Environ* 2017;202:653–63.
- [36] Dong F, Li Y, Wang Z, Ho W-K. Enhanced visible light photocatalytic activity and oxidation ability of porous graphene-like g-C<sub>3</sub>N<sub>4</sub> nanosheets via thermal exfoliation. *Appl Surf Sci* 2015;358:393–403.

- [37] Wang K, Li Q, Liu B, Cheng B, Ho W, Yu J. Sulfur-doped  $g\text{-C}_3\text{N}_4$  with enhanced photocatalytic  $\text{CO}_2$ -reduction performance. *Appl Catal B Environ* 2015;176:177:44–52.
- [38] Liu J, Jia Q, Long J, Wang X, Gao Z, Gu Q. Amorphous NiO as co-catalyst for enhanced visible-light-driven hydrogen generation over  $g\text{-C}_3\text{N}_4$  photocatalyst. *Appl Catal B Environ* 2018;222:35–43.
- [39] Zhu YP, Ren TZ, Yuan ZY. Mesoporous phosphorus-doped  $g\text{-C}_3\text{N}_4$  nanostructured flowers with superior photocatalytic hydrogen evolution performance. *ACS Appl Mater Interfaces* 2015;7:16850–6.
- [40] Yang X, Qian F, Zou G, Li M, Lu J, Li Y, et al. Facile fabrication of acidified  $g\text{-C}_3\text{N}_4/g\text{-C}_3\text{N}_4$  hybrids with enhanced photocatalysis performance under visible light irradiation. *Appl Catal B Environ* 2016;193:22–35.
- [41] Low J, Yu J, Jaroniec M, Wageh S, Al-Ghamdi AA. Heterojunction photocatalysts. *Adv Mater* 2017;29:1601694.
- [42] Carrasco JA, Harvey A, Hanlon D, Lloret V, McAteer D, Sanchis-Gual R, et al. Liquid phase exfoliation of carbonate-intercalated layered double hydroxides. *Chem Commun* 2019;55:3315–8.
- [43] Li C, Wei M, Evans DG, Duan X. Recent advances for layered double hydroxides (LDHs) materials as catalysts applied in green aqueous media. *Catal Today* 2015;247:163–9.
- [44] Mohapatra L, Parida K. A review on the recent progress, challenges and perspective of layered double hydroxides as promising photocatalysts. *J Mater Chem A* 2016;4:10744–66.
- [45] Luo B, Liu G, Wang L. Recent advances in 2D materials for photocatalysis. *Nanoscale* 2016;8:6904–20.
- [46] Zhao Y, Hu H, Yang X, Yan D, Dai Q. Tunable electronic transport properties of 2D layered double hydroxide crystalline microsheets with varied chemical compositions. *Small* 2016;12:4471–6.
- [47] Wang Q, O'Hare D. Recent advances in the synthesis and application of layered double hydroxide (LDH) nanosheets. *Chem Rev* 2012;112:4124–55.
- [48] Ong WJ. 2D/2D graphitic carbon nitride ( $g\text{-C}_3\text{N}_4$ ) heterojunction nanocomposites for photocatalysis: why does face-to-face interface matter? *Front Mater* 2017;4.
- [49] Ni J, Xue J, Xie L, Shen J, He G, Chen H. Construction of magnetically separable NiAl LDH/ $\text{Fe}_3\text{O}_4$ -RGO nanocomposites with enhanced photocatalytic performance under visible light. *Phys Chem Chem Phys* 2018;20:414–21.
- [50] Fan G, Li F, Evans DG, Duan X. Catalytic applications of layered double hydroxides: recent advances and perspectives. *Chem Soc Rev* 2014;43:7040–66.
- [51] Xu ZP, Zhang J, Adebajo MO, Zhang H, Zhou C. Catalytic applications of layered double hydroxides and derivatives. *Appl Clay Sci* 2011;53:139–50.
- [52] He S, An Z, Wei M, Evans DG, Duan X. Layered double hydroxide-based catalysts: nanostructure design and catalytic performance. *Chem Commun* 2013;49:5912–20.
- [53] Tonda S, Kumar S, Bhardwaj M, Yadav P, Ogale S.  $g\text{-C}_3\text{N}_4/\text{NiAl-LDH}$  2D/2D hybrid heterojunction for high-performance photocatalytic reduction of  $\text{CO}_2$  into renewable fuels. *ACS Appl Mater Interfaces* 2018;10:2667–78.
- [54] Wu Y, Wang H, Sun Y, Xiao T, Tu W, Yuan X, et al. Photogenerated charge transfer via interfacial internal electric field for significantly improved photocatalysis in direct Z-scheme oxygen-doped carbon nitrogen/CoAl-layered double hydroxide heterojunction. *Appl Catal B Environ* 2018;227:530–40.
- [55] Abazari R, Mahjoub AR, Sanati S, Rezvani Z, Hou Z, Dai H. Ni-Ti layered double hydroxide@graphitic carbon nitride nanosheet: a novel nanocomposite with high and ultrafast sonophotocatalytic performance for degradation of antibiotics. *Inorg Chem* 2019;58:1834–49.
- [56] Liu J, Li J, Bing X, Ng DHL, Cui X, Ji F, et al. ZnCr-LDH/N-doped graphitic carbon-incorporated  $g\text{-C}_3\text{N}_4$  2D/2D nanosheet heterojunction with enhanced charge transfer for photocatalysis. *Mater Res Bull* 2018;102:379–90.
- [57] Han YY, Lu XL, Tang SF, Yin XP, Wei ZW, Lu TB. Metal-free 2D/2D heterojunction of graphitic carbon nitride/graphdiyne for improving the hole mobility of graphitic carbon nitride. *Adv Energy Mater* 2018;8:1702992.
- [58] Su J, Li GD, Li XH, Chen JS. 2D/2D heterojunctions for catalysis. *Adv Sci* 2019;6:1801702.
- [59] Shi L, Si W, Wang F, Qi W. Construction of 2D/2D layered  $g\text{-C}_3\text{N}_4/\text{Bi}_{12}\text{O}_7/\text{Cl}_2$  hybrid material with matched energy band structure and its improved photocatalytic performance. *RSC Adv* 2018;8:24500–8.
- [60] Shi J, Li S, Wang F, Gao L, Li Y, Zhang X, et al. 2D/2D  $g\text{-C}_3\text{N}_4/\text{MgFe}$  MMO nanosheet heterojunctions with enhanced visible-light photocatalytic  $\text{H}_2$  production. *J Alloys Compd* 2018;769:611–9.
- [61] Li Y, Zhang H, Liu P, Wang D, Li Y, Zhao H. Cross-linked  $g\text{-C}_3\text{N}_4/\text{rGO}$  nanocomposites with tunable band structure and enhanced visible light photocatalytic activity. *Small* 2013;9:3336–44.
- [62] Ong WJ, Tan LL, Chai SP, Yong ST, Mohamed AR. Surface charge modification via protonation of graphitic carbon nitride ( $g\text{-C}_3\text{N}_4$ ) for electrostatic self-assembly construction of 2D/2D reduced graphene oxide (rGO)/ $g\text{-C}_3\text{N}_4$  nanostructures toward enhanced photocatalytic reduction of carbon dioxide to methane. *Nano Energy* 2015;13:757–70.
- [63] Yuan L, Yang MQ, Xu YJ. Tuning the surface charge of graphene for self-assembly synthesis of a  $\text{SnNb}_2\text{O}_6$  nanosheet-graphene (2D–2D) nanocomposite with enhanced visible light photoactivity. *Nanoscale* 2014;6:6335–45.
- [64] Xu Q, Zhu B, Jiang C, Cheng B, Yu J. Constructing 2D/2D  $\text{Fe}_2\text{O}_3/g\text{-C}_3\text{N}_4$  direct Z-scheme photocatalysts with enhanced  $\text{H}_2$  generation performance. *Solar RRL* 2018;2:1800006.
- [65] Fu J, Xu Q, Low J, Jiang C, Yu J. Ultrathin 2D/2D  $\text{WO}_3/g\text{-C}_3\text{N}_4$  step-scheme  $\text{H}_2$ -production photocatalyst. *Appl Catal B Environ* 2019;243:556–65.
- [66] Zhu B, Xia P, Ho W, Yu J. Isoelectric point and adsorption activity of porous  $g\text{-C}_3\text{N}_4$ . *Appl Surf Sci* 2015;344:188–95.
- [67] Yang YJ, Li W. Ultrasonic assisted coating of multiwalled carbon nanotubes with NiFe-layered double hydroxide for improved electrocatalytic oxygen reduction. *J Electroanal Chem* 2018;823:499–504.
- [68] Mao N, Zhou CH, Tong DS, Yu WH, Cynthia Lin CX. Exfoliation of layered double hydroxide solids into functional nanosheets. *Appl Clay Sci* 2017;144:60–78.
- [69] Antonyraj CA, Koilraj P, Kannan S. Synthesis of delaminated LDH: a facile two step approach. *Chem Commun* 2010;46:1902–4.
- [70] Zhang J, Chen Y, Wang X. Two-dimensional covalent carbon nitride nanosheets: synthesis, functionalization, and applications. *Energy Environ Sci* 2015;8:3092–108.
- [71] Zhang X, Xie X, Wang H, Zhang J, Pan B, Xie Y. Enhanced photoresponsive ultrathin graphitic-phase  $\text{C}_3\text{N}_4$  nanosheets for bioimaging. *J Am Chem Soc* 2013;135:18–21.
- [72] Hong J, Zhang W, Wang Y, Zhou T, Xu R. Photocatalytic reduction of carbon dioxide over self-assembled carbon nitride and layered double hydroxide: the role of carbon dioxide enrichment. *ChemCatChem* 2014;6:2315–21.
- [73] Nayak S, Mohapatra L, Parida K. Visible light-driven novel  $g\text{-C}_3\text{N}_4/\text{NiFe-LDH}$  composite photocatalyst with enhanced photocatalytic activity towards water oxidation and reduction reaction. *J Mater Chem A* 2015;3:18622–35.
- [74] Chu X, Wang J, Bai L, Dong Y, Sun W, Zhang W. Trimethylamine and ethanol sensing properties of  $\text{NiGa}_2\text{O}_4$  nano-materials prepared by co-precipitation method. *Sensors Actuators B Chem* 2018;255:2058–65.
- [75] Moghadam AK, Mirzaee O, Shokrollahi H, Lavasani SANH. Magnetic and morphological characterization of bulk  $\text{Bi}_2\text{Fe}_4\text{O}_9$  derived by reverse chemical co-precipitation: a comparative study of different sintering methods. *Ceram Int* 2019;45:8087–94.
- [76] Niu J, Qian H, Liu J, Liu H, Zhang P, Duan E. Process and mechanism of toluene oxidation using  $\text{Cu}_{1-y}\text{Mn}_2\text{Ce}_y\text{O}_x/\text{sepiolite}$  prepared by the co-precipitation method. *J Hazard Mater* 2018;357:332–40.
- [77] Theiss FL, Ayoko GA, Frost RL. Synthesis of layered double hydroxides containing  $\text{Mg}^{2+}$ ,  $\text{Zn}^{2+}$ ,  $\text{Ca}^{2+}$  and  $\text{Al}^{3+}$  layer cations by co-precipitation methods—a review. *Appl Surf Sci* 2016;383:200–13.
- [78] Arif M, Yasin G, Shakeel M, Fang X, Gao R, Ji S, et al. Coupling of bifunctional CoMn-layered double hydroxide@graphitic  $\text{C}_3\text{N}_4$  nanohybrids towards efficient photoelectrochemical overall water splitting. *Chem Asian J* 2018;13:1045–52.
- [79] Yuan X, Li W. Graphitic- $\text{C}_3\text{N}_4$  modified ZnAl-layered double hydroxides for enhanced photocatalytic removal of organic dye. *Appl Clay Sci* 2017;138:107–13.
- [80] Meng LY, Wang B, Ma MG, Lin KL. The progress of microwave-assisted hydrothermal method in the synthesis of functional nanomaterials. *Mater Today Chem* 2016;1–2:63–83.
- [81] Akbarzadeh R, Fung CSL, Rather RA, Lo IMC. One-pot hydrothermal synthesis of  $g\text{-C}_3\text{N}_4/\text{Ag/AgCl/BiVO}_4$  micro-flower composite for the visible light degradation of ibuprofen. *Chem Eng J* 2018;341:248–61.
- [82] Xu Y, Liu T, Li Y, Liu Y, Ge F. Nanostructure design and catalytic performance of Mo/ZnAl-LDH in cationic orchid X-BL removal. *Materials* 2018;11:2390.
- [83] Liu X, Liang J, Song X, Yang H, Li X, Dai H, et al. Enhanced water dissociation performance of graphitic- $\text{C}_3\text{N}_4$  assembled with ZnCr-layered double hydroxide. *Chem Eng J* 2018;337:560–6.
- [84] Yazdani D, Zinatizadeh AA, Joshaghani M. Organic-inorganic Z-scheme  $g\text{-C}_3\text{N}_4$ -NiTi-layered double hydroxide films for photocatalytic applications in a fixed-bed reactor. *J Ind Eng Chem* 2018;63:65–72.
- [85] Demazeau G. Solvothermal reactions: an original route for the synthesis of novel materials. *J Mater Sci* 2008;43:2104–14.
- [86] Lai J, Niu W, Luque R, Xu G. Solvothermal synthesis of metal nanocrystals and their applications. *Nano Today* 2015;10:240–67.
- [87] Dantelle G, Testemale D, Homeyer E, Cantarano A, Kodjikian S, Dujardin C, et al. A new solvothermal method for the synthesis of size-controlled YAG:Ce single-nanocrystals. *RSC Adv* 2018;8:26857–70.
- [88] Zhang L, Li L, Sun X, Liu P, Yang D, Zhao X. ZnO-layered double hydroxide@graphitic carbon nitride composite for consecutive adsorption and photodegradation of dyes under UV and visible lights. *Materials* 2016;9:927.
- [89] Ahmed N, Morikawa M, Izumi Y. Photocatalytic conversion of carbon dioxide into methanol using optimized layered double hydroxide catalysts. *Catal Today* 2012;185:263–9.
- [90] Wang C, Zhang X, Xu Z, Sun X, Ma Y. Ethylene glycol intercalated cobalt/nickel layered double hydroxide nanosheet assemblies with ultrahigh specific capacitance: structural design and green synthesis for advanced electrochemical storage. *ACS Appl Mater Interfaces* 2015;7:19601–10.
- [91] Shakeel M, Arif M, Yasin G, Li B, Khan HD. Layered by layered Ni-Mn-LDH/ $g\text{-C}_3\text{N}_4$  nanohybrid for multi-purpose photo/electrocatalysis: morphology controlled strategy for effective charge carriers separation. *Appl Catal B Environ* 2019;242:485–98.
- [92] Arif M, Yasin G, Shakeel M, Mushtaq MA, Ye W, Fang X, et al. Hierarchical CoFe-layered double hydroxide and  $g\text{-C}_3\text{N}_4$  heterostructures with enhanced bifunctional photo/electrocatalytic activity towards overall water splitting. *Mater Chem Front* 2019;3:520–31.
- [93] Li C, Wei M, Evans DG, Duan X. Layered double hydroxide-based nanomaterials as highly efficient catalysts and adsorbents. *Small* 2014;10:4469–86.
- [94] Yang Z, Wang F, Zhang C, Zeng G, Tan X, Yu Z, et al. Utilization of LDH-based materials as potential adsorbents and photocatalysts for the decontamination of dyes wastewater: a review. *RSC Adv* 2016;6:79415–36.
- [95] Van Vaerenbergh B, De Vlieger K, Claeys K, Vanhoutte G, De Clercq J, Vermeir P, et al. The effect of the hydrothermal structure and nanoparticle size on the catalytic performance of supported palladium nanoparticle catalysts in Suzuki cross-coupling. *Appl Catal A Gen* 2018;550:236–44.
- [96] Patnaik S, Sahoo DP, Mohapatra L, Marthia S, Parida K. ZnCr<sub>2</sub>O<sub>4</sub>@ZnO/ $g\text{-C}_3\text{N}_4$ : a triple-junction nanostructured material for effective hydrogen and oxygen evolution under visible light. *Energy Technol* 2017;5:1687–701.



- [97] Di G, Zhu Z, Huang Q, Zhang H, Zhu J, Qiu Y, et al. Targeted modulation of g-C<sub>3</sub>N<sub>4</sub> photocatalytic performance for pharmaceutical pollutants in water using ZnFe-LDH derived mixed metal oxides: structure-activity and mechanism. *Sci Total Environ* 2019;650:1112–21.
- [98] Wang R, Pan K, Han D, Jiang J, Xiang C, Huang Z, et al. Solar-driven H<sub>2</sub>O<sub>2</sub> generation from H<sub>2</sub>O and O<sub>2</sub> using earth-abundant mixed-metal oxide@carbon nitride photocatalysts. *ChemSusChem* 2016;9:2470–9.
- [99] Muresanu M, Radu T, Andrei R-D, Darie M, Carja G. Green synthesis of g-C<sub>3</sub>N<sub>4</sub>/CuONP/LDH composites and derived g-C<sub>3</sub>N<sub>4</sub>/MMO and their photocatalytic performance for phenol reduction from aqueous solutions. *Appl Clay Sci* 2017;141:1–12.
- [100] Lan M, Fan G, Yang L, Li F. Enhanced visible-light-induced photocatalytic performance of a novel ternary semiconductor coupling system based on hybrid Zn-in mixed metal oxide/g-C<sub>3</sub>N<sub>4</sub> composites. *RSC Adv* 2015;5:5725–34.
- [101] Gao Z, Sasaki K, Qiu X. Structural memory effect of Mg–Al and Zn–Al layered double hydroxides in the presence of different natural humic acids: process and mechanism. *Langmuir* 2018;34:5386–95.
- [102] Peng F, Wang D, Cao H, Liu X. Loading 5-fluorouracil into calcined Mg/Al layered double hydroxide on AZ31 via memory effect. *Mater Lett* 2018;213:383–6.
- [103] Yuan X, Jing Q, Chen J, Li L. Photocatalytic Cr(VI) reduction by mixed metal oxide derived from ZnAl layered double hydroxide. *Appl Clay Sci* 2017;143:168–74.
- [104] Li D, Lu M, Cai Y, Cao Y, Zhan Y, Jiang L. Synthesis of high surface area MgAl<sub>2</sub>O<sub>4</sub> spinel as catalyst support via layered double hydroxides-containing precursor. *Appl Clay Sci* 2016;132–133:243–50.
- [105] Luo B, Song R, Jing D. ZnCr LDH nanosheets modified graphitic carbon nitride for enhanced photocatalytic hydrogen production. *Int J Hydrog Energy* 2017;42:23427–36.
- [106] Salehi G, Abazari R, Mahjoub AR. Visible-light-induced graphitic-C<sub>3</sub>N<sub>4</sub>@Nickel–aluminum layered double hydroxide nanocomposites with enhanced photocatalytic activity for removal of dyes in water. *Inorg Chem* 2018;57:8681–91.
- [107] Li K, Peng B, Peng T. Recent advances in heterogeneous photocatalytic CO<sub>2</sub> conversion to solar fuels. *ACS Catal* 2016;6:7485–527.
- [108] Jo W-K, Tonda S. Novel CoAl-LDH/g-C<sub>3</sub>N<sub>4</sub>/RGO ternary heterojunction with notable 2D/2D/2D configuration for highly efficient visible-light-induced photocatalytic elimination of dye and antibiotic pollutants. *J Hazard Mater* 2019;368:778–87.
- [109] Nayak S, Parida KM. Dynamics of charge-transfer behavior in a plasmon-induced quasi-type-II p–n/n–n dual heterojunction in Ag@Ag<sub>3</sub>PO<sub>4</sub>/g-C<sub>3</sub>N<sub>4</sub>/NiFe LDH nanocomposites for photocatalytic Cr(VI) reduction and phenol oxidation. *ACS Omega* 2018;3:7324–43.
- [110] Nayak S, Parida KM. Deciphering Z-scheme charge transfer dynamics in heterostructure NiFe-LDH/N-rGO/g-C<sub>3</sub>N<sub>4</sub> nanocomposite for photocatalytic pollutant removal and water splitting reactions. *Sci Rep* 2019;9:2458.
- [111] Tonda S, Jo W-K. Plasmonic Ag nanoparticles decorated NiAl-layered double hydroxide/graphitic carbon nitride nanocomposites for efficient visible-light-driven photocatalytic removal of aqueous organic pollutants. *Catal Today* 2018;315:213–22.
- [112] Low J, Jiang C, Cheng B, Wageh S, Al-Ghamdi AA, Yu J. A review of direct Z-scheme photocatalysts. *Small Methods* 2017;1:1700080.
- [113] Zhao Y, Zhao Y, Waterhouse GIN, Zheng L, Cao X, Teng F, et al. Layered-double-hydroxide nanosheets as efficient visible-light-driven photocatalysts for dinitrogen fixation. *Adv Mater* 2017;29:1703828.
- [114] Li Y, Jin R, Xing Y, Li J, Song S, Liu X, et al. Macroscopic foam-like holey ultrathin g-C<sub>3</sub>N<sub>4</sub> nanosheets for drastic improvement of visible-light photocatalytic activity. *Adv Energy Mater* 2016;6:1601273.
- [115] Wang Q, Wang W, Zhong L, Liu D, Cao X, Cui F. Oxygen vacancy-rich 2D/2D BiOCl-g-C<sub>3</sub>N<sub>4</sub> ultrathin heterostructure nanosheets for enhanced visible-light-driven photocatalytic activity in environmental remediation. *Appl Catal B Environ* 2018;220:290–302.